REPORT DOCUMENTATION PAGE	Form Approved OMB NO. 0704-0188

The public reporting burden for this collection of information is estimated to average 1 hour per response, including the time for reviewing instructions, searching existing data sources, gathering and maintaining the data needed, and completing and reviewing the collection of information. Send comments regarding this burden estimate or any other aspect of this collection of information, including suggesstions for reducing this burden, to Washington Headquarters Services, Directorate for Information Operations and Reports, 1215 Jefferson Davis Highway, Suite 1204, Arlington VA, 22202-4302. Respondents should be aware that notwithstanding any other provision of law, no person shall be subject to any oenalty for failing to comply with a collection of information if it does not display a currently valid OMB control number.
PLEASE DO NOT RETURN YOUR FORM TO THE ABOVE ADDRESS.

1. REPORT DATE (DD-MM-YYYY)	2. REPORT TYPE	3. DATES COVERED (From - To)
12-01-2011	Final Report	1-Mar-2005 - 30-Jun-2009

4. TITLE AND SUBTITLE	5a. CONTRACT NUMBER
Design optimization and characterization of helicoidal composites with enhanced impact resistance	W911NF-05-1-0065
	5b. GRANT NUMBER
	5c. PROGRAM ELEMENT NUMBER
	611102

6. AUTHORS	5d. PROJECT NUMBER
Krishnaswamy RAVI-CHANDAR	5e. TASK NUMBER
	5f. WORK UNIT NUMBER

7. PERFORMING ORGANIZATION NAMES AND ADDRESSES	8. PERFORMING ORGANIZATION REPORT NUMBER
University of Texas at Austin The University of Texas at Austin 101 East 27th Street Austin, TX 78712 -1500	

9. SPONSORING/MONITORING AGENCY NAME(S) AND ADDRESS(ES)	10. SPONSOR/MONITOR'S ACRONYM(S)
U.S. Army Research Office P.O. Box 12211 Research Triangle Park, NC 27709-2211	ARO
	11. SPONSOR/MONITOR'S REPORT NUMBER(S)
	47003-EG.1

12. DISTRIBUTION AVAILIBILITY STATEMENT

Approved for Public Release; Distribution Unlimited

13. SUPPLEMENTARY NOTES

The views, opinions and/or findings contained in this report are those of the author(s) and should not contrued as an official Department of the Army position, policy or decision, unless so designated by other documentation.

14. ABSTRACT

The impact response of helicoidal composites was evaluated under low and high speed impact conditions. Helicoidal composites in which the ply-to-ply angle mismatch is minimized to 10 degrees were fabricated out off unidirectional carbon-epoxy lamina and plain-weave glass-epoxy lamina. These laminates were shown to be significantly superior to standard lay-ups under quasi-static loading conditions. Low speed impact tests were used to determine the suitability o numerical simulations (including cohesive zone modeling) to capture the dynamic

15. SUBJECT TERMS

helicoidal, bio-inspired composite, impact response

16. SECURITY CLASSIFICATION OF:			17. LIMITATION OF ABSTRACT	15. NUMBER OF PAGES	19a. NAME OF RESPONSIBLE PERSON
a. REPORT	b. ABSTRACT	c. THIS PAGE			Krishnaswamy Ravi-Chandar
UU	UU	UU	UU		19b. TELEPHONE NUMBER
					512-471-4213

Standard Form 298 (Rev 8/98)
Prescribed by ANSI Std. Z39.18

Report Title

Design optimization and characterization of helicoidal composites with enhanced impact resistance

ABSTRACT

The impact response of helicoidal composites was evaluated under low and high speed impact conditions. Helicoidal composites in which the ply-to-ply angle mismatch is minimized to 10 degrees were fabricated out off unidirectional carbon-epoxy lamina and plain-weave glass-epoxy lamina. These laminates were shown to be significantly superior to standard lay-ups under quasi-static loading conditions. Low speed impact tests were used to determine the suitability o numerical simulations (including cohesive zone modeling) to capture the dynamic response of helicoidal plates subjected to transverse impact. High speed impact tests were used to determine the ballistic limit; v_50 values in the range of 150 to 200 m/s were obtained on laminates that were about 0.25 in thick. While a 25% improvement was found in the v_50 of the helicoidal composite, the performance just beyond v_50 was very similar to the standard lay-up. The addition of a more ductile polymer layer - such as polycarbonate - was shown to improve the performance significantly.

List of papers submitted or published that acknowledge ARO support during this reporting period. List the papers, including journal references, in the following categories:

(a) Papers published in peer-reviewed journals (N/A for none)

Number of Papers published in peer-reviewed journals: 0.00

(b) Papers published in non-peer-reviewed journals or in conference proceedings (N/A for none)

Scott Walker, Helicoidal Composites, MS Thesis, University of Texas at Austin

Number of Papers published in non peer-reviewed journals: 1.00

(c) Presentations

"Impact response of helicoidal composites: Experiments and Models", 17th US Army Symposium on Solid Mechanics, Baltimore, MD, April 2007

Number of Presentations: 1.00

Non Peer-Reviewed Conference Proceeding publications (other than abstracts):

Number of Non Peer-Reviewed Conference Proceeding publications (other than abstracts):   0

Peer-Reviewed Conference Proceeding publications (other than abstracts):

Number of Peer-Reviewed Conference Proceeding publications (other than abstracts):   0

(d) Manuscripts

Ballistic response of bio-inspired helicoidal composite,
in preparation.

Number of Manuscripts: 1.00

Patents Submitted

Patents Awarded

Awards

Graduate Students

NAME	PERCENT SUPPORTED	
Scott Walker	1.00	
Federico Gallo	0.30	
FTE Equivalent:	**1.30**	
Total Number:	**2**	

Names of Post Doctorates

NAME	PERCENT_SUPPORTED
FTE Equivalent:	
Total Number:	

Names of Faculty Supported

NAME	PERCENT_SUPPORTED	National Academy Member
Krishnaswamy Ravi-Chandar	0.10	No
FTE Equivalent:	**0.10**	
Total Number:	**1**	

Names of Under Graduate students supported

NAME	PERCENT_SUPPORTED
FTE Equivalent:	
Total Number:	

Student Metrics
This section only applies to graduating undergraduates supported by this agreement in this reporting period

The number of undergraduates funded by this agreement who graduated during this period: 0.00

The number of undergraduates funded by this agreement who graduated during this period with a degree in science, mathematics, engineering, or technology fields:...... 0.00

The number of undergraduates funded by your agreement who graduated during this period and will continue to pursue a graduate or Ph.D. degree in science, mathematics, engineering, or technology fields:...... 0.00

Number of graduating undergraduates who achieved a 3.5 GPA to 4.0 (4.0 max scale):...... 0.00

Number of graduating undergraduates funded by a DoD funded Center of Excellence grant for Education, Research and Engineering:...... 0.00

The number of undergraduates funded by your agreement who graduated during this period and intend to work for the Department of Defense 0.00

The number of undergraduates funded by your agreement who graduated during this period and will receive scholarships or fellowships for further studies in science, mathematics, engineering or technology fields:...... 0.00

Names of Personnel receiving masters degrees

NAME

Scott Walker

Total Number: 1

Names of personnel receiving PHDs

NAME

Total Number:

Names of other research staff

NAME   PERCENT_SUPPORTED

FTE Equivalent:
Total Number:

Sub Contractors (DD882)

Inventions (DD882)

Scientific Progress

The impact response of helicoidal composites was evaluated under low and high speed impact conditions. Helicoidal composites in which the ply-to-ply angle mismatch is minimized to 10 degrees were fabricated out off unidirectional carbon-epoxy lamina and plain-weave glass-epoxy lamina. These laminates were shown to be significantly superior to standard lay-ups under quasi-static loading conditions. Low speed impact tests were used to determine the suitability o numerical simulations (including cohesive zone modeling) to capture the dynamic response of helicoidal plates subjected to transverse impact. High speed impact tests were used to determine the ballistic limit; v_{50} values in the range of 150 to 200 m/s were obtained on laminates that were about 0.25 in thick. While a 25% improvement was found in the v_{50} of the helicoidal composite, the performance just beyond v_{50} was very similar to the standard lay-up. The addition of a more ductile polymer layer - such as polycarbonate - was shown to improve the performance significantly.

Technology Transfer

IMPACT RESPONSE OF HELICOIDAL

COMPOSITES

January 2011

Final report to the

ARMY RESEARCH OFFFICE

W911NF-05-1-0065

Krishnaswamy RAVI-CHANDAR

Center for the Mechanics of Solids, Structures and Materials

THE UNIVERSITY OF TEXAS AT AUSTIN

TABLE OF CONTENTS

LIST OF FIGURES

LIST OF TABLES

1. Introduction and Background

Composite materials have a high strength to weight ratio and thus possess significant potential for application in high-performance, lightweight structures. However, since these laminated structures develop significant interlaminar shear stresses and are quite weak across the lamina, delamination, transverse matrix cracks and other failure modes intervene and reduce the effective strength of the composites to levels much smaller than their true potential. Understanding these failure modes is essential not only in determining appropriate allowable loads on composite structures, but also in designing improved materials with better properties.

There have been numerous experiments and models generated to understand and predict the phenomenon of delamination in composites (the bibliography lists a selected few publications that deal with the issue; Science Citation Index indicates that there are at least 2000 references on the subject of composite delamination). In very early work, Chai *et al*., (1981, 1983) demonstrated that delamination was a crucial limiting factor for composites under low-speed impact. The role of interlaminar stresses and free-edge delamination in limiting the strength of composite materials has also been recognized for quite some time; the early work of Pagano (1978) set the stage for intensive investigations in this area. Based on numerous experimental investigations that revealed the mechanisms of deformation and failure in composites, micromechanics based constitutive models have been developed that capture the mechanical behavior of composite materials; a good concise summary of progress in this area can be found in the article by Dvorak (2000). This article also provides a listing of open issues in composites that require further attention. Specifically with reference to delamination, damage and failure under dynamic loading conditions, Dvorak stresses the need for further experimental and modeling research; ideas such as selective reinforcement, improved adhesion characteristics and generation of residual stresses are suggested for improving the delamination and damage resistance in composites.

Recognizing that delamination is driven by interlaminar stresses and the weak bond across the laminae, much work has been done aimed at determining the role of the lamination in dictating the damage resistance of composites under quasi-static and dynamic loading. For example, Tao and Sun (1998) performed an experiment to investigate the interlaminar fracture behavior and toughness of $0°/\theta$ interface with $\theta = 30°$, $45°$, $60°$ and $90°$. They found that the interlaminar toughness decreases as the off-axis θ angle increases and remains constant as θ changes from $15°$

to 90º. Hsiao *et al*., (1998) studied the effect of strain rate and the fiber orientation on the mechanical properties of thick carbon/epoxy composite materials. They observed that the strength and ultimate strain values increased as strain rate increased and that the specimen with transverse direction fiber has higher stiffness than the longitudinal direction. An impact analysis of laminated composite performed by Liou (1997) found that for the anisotropic laminated plate, higher stresses exist in the direction having higher stiffness and that the delamination cracks are caused by the interlaminar stresses.

Christensen and DeTeresa (1992) showed that the edge singularities that arise in laminated composites either vanish or are minimized for certain special laminations. This is a very interesting observation but only applies for special orientations of the loading; however, the underlying idea that through proper choice of fiber architecture, one may influence the development of damage in composite materials is very important. This idea has been followed up in many analytical investigations, but to our knowledge, not in experimental investigations. Suvorov and Dvorak (2001a) have explored the possibility of prestressing selected lamina in order to control the development of free-edge stresses; this is somewhat akin to prestressing concrete with rebar, with the additional influence of material anisotropy. They suggest that by selectively prestressing certain layers prior to matrix infiltration/consolidation and then releasing upon curing, large compressive prestress can be generated in the matrix layers thereby minimizing matrix cracking and delamination. Sovorov and Dvorak (2001b) also indicate that designs of such prestressed laminate/ceramic plate assembly can also introduce significant compressive stresses of the order of 600 MPa to 1 GPa in the ceramic layer. These models raise interesting possibilities for enhancing the mechanical properties of composite materials; the helicoidal composite that is the focus of this study is a development along these lines.

Many investigators have employed through-thickness reinforcement as a way of mitigating the delamination problem. The reinforcement can be achieved by many methods such as stitching, braiding, z-fibers/z-rods, fiber waviness or adhesive strips. The experiments performed by Rugg *et al.* (1998, 2002) found that the through-thickness reinforcement by z-rods raised the critical stress for delamination significantly. For the through-thickness reinforced structure, when the delamination cracks initiate and propagate, the z-fibers or reinforcements stop the crack at each location. The applied load must then increase to the strength limit of the reinforcement before the

delamination cracks can restart propagation until they encounter the next reinforcement. This cycle repeats until reaching the last reinforcement and total failure occurs. Therefore, the load and displacement diagram presents a stepped line instead of linear line in ordinary laminate, but the ultimate load is significantly increased. In very recent work Baucom and Zikry (2003), Bahei-El-Din and Zikry (2003) and Zikry et al (2003) have explored the mechanism of failure in 2D, 3D woven composites and 3D woven porous composites and utilized finite element modeling to generate constitutive modeling of the failure in these composites.

We have taken an approach that combines the two strategies discussed above. We have demonstrated (Apicartthabrut and Ravi-Chandar, 2006) in carbon-epoxy systems that by altering the lay-up to a helicoidal structure, significant improvements in the strength and impact resistance can be achieved (see summary in the next section for details). In addition, by providing through-thickness reinforcement by z-pinning with staple, further significant improvements in delamination resistance and penetration resistance was demonstrated. The helicoidal lay-up with through-thickness reinforcement can be optimized to control the residual interlaminar stresses, to inhibit the development of transverse cracks, to increase the delamination toughness, and as a consequence to improve the static strength and dynamic impact resistance of the composite. In principle, a similar enhancement is possible in glass-epoxy systems, either in laminated or woven forms. Providing such enhancements in the strength and impact resistance for the glass-epoxy systems is the main motivation of this work. We first provide a summary of accomplishments under previous ARO funded research that lead to the development of the helicoidal composite in and then describe the results of the work performed under the current grant.

2. Summary of Accomplishments of Previous ARO Funded Research

In a previously study, Apichartthabrut and Ravi-Chandar, (2006) developed a new design for composite materials that is based to some extent on imitating biological composites. Many natural composites in plants and animals form in a helicoidal structure (Neville, 1993); adopting this strategy to engineered composites, *we have fabricated composite panels with a helicoidal architecture* (Apichartthabrut and Ravi-Chandar, 2003). Design of this helicoidal structure and the fabrication method are discussed in Appendices A and B respectively. The helicoidal composite was generated by laying 40 plies at 10 degree increments, resulting in two turns of the helix with four additional layers oriented along the zero direction at the middle. The helicoidal structure provides a nearly continuous grading of the in-plane stiffness in the thickness direction and therefore reduces the interlaminar shear stresses significantly. In addition, favorable thermal residual stresses are built into the plate during fabrication. Plate bending tests were performed on circular plates clamped at the boundaries and loaded by a spherical punch at the center. A comparison of the response of a 40 layer helicoidal architecture with a 24 layer [+45/-45] composite plate (representative of a plain weave architecture) in bending tests is shown in Fig. 1; the two composites were nearly of the same total thickness, but all
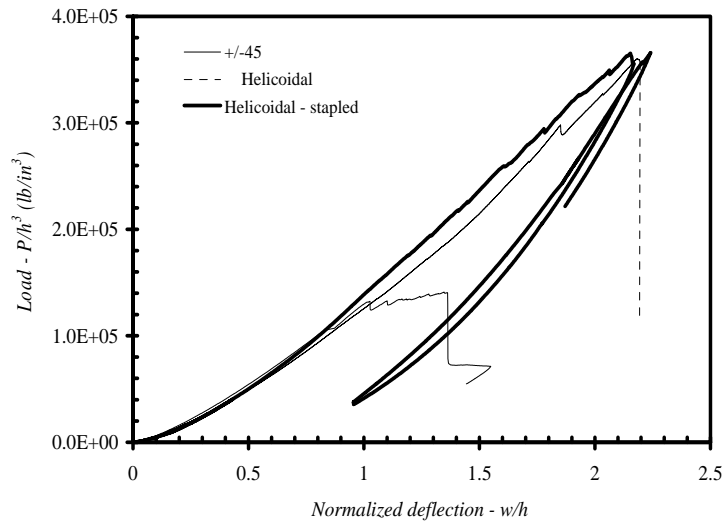
Figure 1. Comparison of the load-deflection diagram for the helicoidal composite and the ± 45° composite.

quantities are plotted normalized with the appropriate thickness. The nonlinearity observed in all of these tests is due to the large indentation of the plate by the spherical punch used to apply the loads. Due to the discrete nature of the ± 45° composite, it developed cracks in a catastrophic manner and delaminated across the entire plate diameter after a deflection of one plate thickness. On the other hand, the graded nature of the helicoids allowed for a reduction in the interlaminar

shear stresses and hence delamination was delayed until much larger plate deflections and a corresponding increase in the load carrying capacity.

In spite of the graded nature of the helicoidal composites, once the delamination was initiated, it grew catastrophically resulting in a significant load drop. This is because delamination is controlled by the interlayer matrix and this is not affected significantly by the graded architecture; therefore improvements in the fracture energies cannot be obtained by altering the in-plane architecture alone. This has commonly been approached through a three dimensional fiber architecture obtained either by a woven fabric reinforcement or through cross stitching or stapling; we adopted the stapling approach as a first step (Rugg *et al*., 1998). The helicoidal composite was stapled through in an axisymmetric pattern with the z-reinforcement provided by steel staples of cross sectional area 0.00125 in^2 with approximately 11 staples per in^2; as a result, roughly 1.35% of the area is covered by the staples. The staples are introduced into the composite before curing; during insertion, the easy mobility of the fibers results in very little damage to the fibers; they simply move aside to allow the staple to penetrate. The influence of the staples on the composite toughness was examined in a double cantilever beam (DCB) test. The response of the stapled plate under bending is compared with the unstitched and +/-45 plates in Fig. 1. Both helicoidal composites – unstitched and stitched – exhibit a similar response until a deflection of about twice the plate thickness. However, in contrast to the unstitched composite, the stitched composite did not exhibit catastrophic delamination. Clearly a high unloading stiffness can be seen in Fig. 1 indicating that this specimen is capable of withstanding a much greater ultimate load. Crushing damage localized at the point of load application, but there was no global delamination.

The impact response of the helicoidal composite was also examined in comparison with the ± 45° specimen. A steel projectile with a rounded nose was propelled from an air gun at a speed of about 55 m/s; the total impact energy was about 700 J. The resulting damage is shown in Fig. 2. While the ± 45° specimen exhibited complete penetration as seen in Fig.2a, the helicoidal composite indicated only a localized indentation (Fig. 2b). It is suspected that there might be some internal delaminations, but this could not be verified. In the z-reinforced helicoidal composite, even this localized damage was not visible. From this demonstration, it is clear that the helicoidal architecture possess significant advantages in terms of strength and damage resistance. Of course, we did not make any attempt at optimization of either the architecture or the z-reinforcement patter

5

and methodology. We have merely shown the promise of the helicoidal architecture in enhancing the strength and impact resistance of composites. In very recent work, Cheng et al (2011) have examined many variations of the helicoidal structure and demonstrated the superior strength of this structure. We now continue to examine this development in its logical next steps – applying the methodology to glass-epoxy systems of interest to Army hardware, optimizing the fiber architecture and the z-reinforcement methodology, and characterizing the static and dynamic properties of the resulting composite.

3. Impact Response of Helicoidal Composites

A relatively new use for composites is in the area of high-speed projectile impact. Some cloth-like composite materials (Kevlar) can be made into bullet-proof vests. Stiffer carbon fiber plates have even begun replacing heavy steel shielding in light armored vehicles. Improving the ballistic capabilities of these carbon and glass fiber plates is the focus of this work. To increase a material's ballistic resistance it is necessary to increase the amount of energy absorbed by the material during the impact event. This is typically quantified by a value known as the ballistic limit, V_{50}, of the material; the ballistic limit is the lowest velocity at which a standardized projectile can impact a target and obtain complete penetration.

With fiber composites there are several energy absorption mechanisms: matrix fracture, fiber deformation and breakage, friction, fiber/matrix debonding and delamination. Studies described by Harel et al (2000) showed that delamination accounted for a major portion of the absorbed energy, with fiber strain and matrix fracture also having significant contributions. Delamination is caused by high inter laminar stresses as well as a low through-thickness debonding resistance. Inter laminar stresses develop when there is a sizable difference in the elastic properties of two successive lamina. Usually this strength discrepancy comes from a large change in the fiber directions across two neighboring lamina. Jianxin and Sun (1998) showed that inter laminar toughness decreases as the fiber angle between lamina increases from 0° to 15°. At angles greater than 15° the interlaminar toughness was approximately constant. The helicoidal design makes use of these findings by rotating the fiber direction of each subsequent lamina by only 10°. A smaller rotation would have resulted in a very thick laminate, while a larger rotation would have resulted in a decreased inter laminar toughness as described earlier. The exact layup of the helicoid is [0/10/20/30/40/50/60/70/80/90/100/110/120/130/140/150/160/170/(0)$_2$]$_s$. More energy should be needed to debond this laminate than a laminate with equal thickness composed entirely of layers oriented only at right angles to each other.

In order to increase the through-thickness debonding resistance of a laminate, many researchers have used reinforcement techniques that act perpendicular to the plane of the laminate. Some of these methods involve stitching, braiding, or weaving fibers together. Other methods use adhesive strips placed in between lamina. Cox et al (2002) showed that through-thickness reinforcement by z-rods increased the level of energy needed to cause a

delamination. To achieve this type of reinforcement the laminate is literally stapled together. Z-rod reinforcement not only increases the critical stress for delamination, but also can act as a crack arrestment device. Once a crack has been initiated in the matrix material it does not take a significant increase in energy to propagate through the matrix. However, if the crack intersects a z-direction rod it will be stopped until the applied load is enough to pull out or break the rod. This cycle will be repeated each time the crack intersects a new rod thereby making the load vs displacement plot into a stepped line. Fiber strain also plays a significant role in the energy absorption of composite materials. In this research the effect of placing thin layers of polycarbonate between carbon fiber layers is investigated. These isotropic materials can experience high levels of strain without fracture, and may absorb enough energy to delay the onset of fiber break.

3.1. Numerical Simulation of Impact Response of a Helicoidal Composite

Several computer models were made using ABAQUS finite element tools to simulate the dynamic impact event on a clamped circular plate in order to explore the design of the helicoidal composite. To replicate the clamped plate with finite elements only the cut-out area is needed. Therefore, the model considered is a 280 mm diameter disc; each composite layer is 0.17 mm thick. There are a total of 40 layers, making the entire model 6.8 mm thick. Each model is completely restrained against displacements and rotations around the edges in order to reproduce a clamped boundary condition. The projectile is represented as a rigid body that has the same dimensions and mass as the real projectile. The projectile velocity can be modified to match the velocity produced in each experiment. All of the models use the same orthotropic material properties for the elastic elements. In the simplest elastic model all of the composite layers remain intact and completely bonded during impact. In more representative models, a cohesive interaction allows for delaminations to occur between layers. There are separate cohesive models which simulate either the high speed or the low speed experiment and these will be discussed below. Two different layup designs were compared in this part of the study. A standard layup with a $[(0/90)_{19}/0]_s$ (referred to as a 0/90) stacking sequence is compared to a helicoidal layup with a $[0/10/20/30/40/50/60/70/80/90/100/110/120/130/140/150/160/170/(0)_2]_s$ stacking sequence.

3.1.1. Elastic Model

The elastic model contains 909,760 C3D8R elements and 926,640 nodes. C3D8R elements are 3 dimensional, 8 node, brick elements that use a reduced integration algorithm to improve computation time and hour glass control to prevent locking. Each composite layer is modeled with 4 elements through its thickness. The mesh is densest at the point of impact (center) and becomes coarser toward the periphery. An overview of the model is shown in Figure 3. The element material properties are given in Table 1.

Table 1. Elastic constants for the composite lamina

Property	E_1 (GPa)	E_2 (GPa)	E_3 (GPa)	ν_1	ν_2	ν_3	G_1 (GPa)	G_2 (GPa)	G_3 (GPa)
	125	12.4	12.4	0.3	0.3	0.3	4.4	4.4	4.4

For the first analysis, the projectile velocity was set to 48.6 m/s in order to match the best set of results from the low speed, high projectile mass experiments to be discussed later. Figure 4 shows
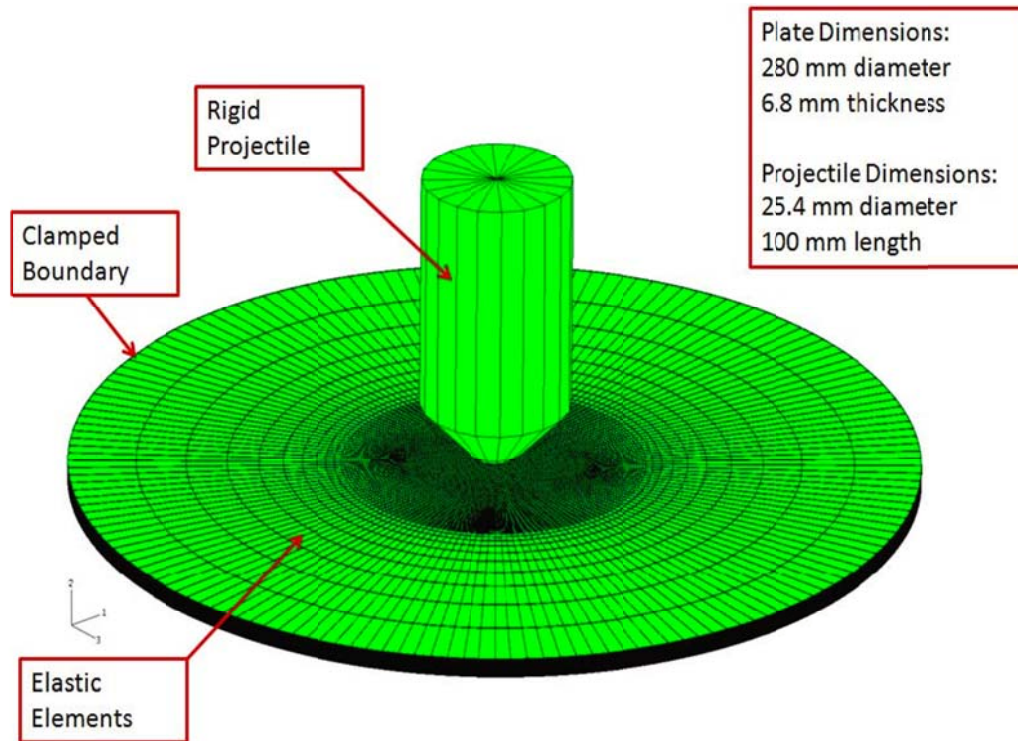
Figure 3. ABAQUS Finite Element Model

9

the out-of-plane displacement of the backside 45.0 µs after impact for the 0/90 and helicoid. The maximum displacement at this time is 1.5 mm and is very similar in both plates. The corresponding principal stress variation is shown in Figure 5. The peak maximum principal stress is about 3 GPa. Since the flexural strength of the NCT304-1 Carbon Epoxy is only 1.68 GPa the plates will have failed several microseconds before this time; however, this simple model does not take material failure into account. The purpose of the elastic model is to compare the helicoidal fiber layup to the standard 0/90 layup; it can be observed that the response is similar.
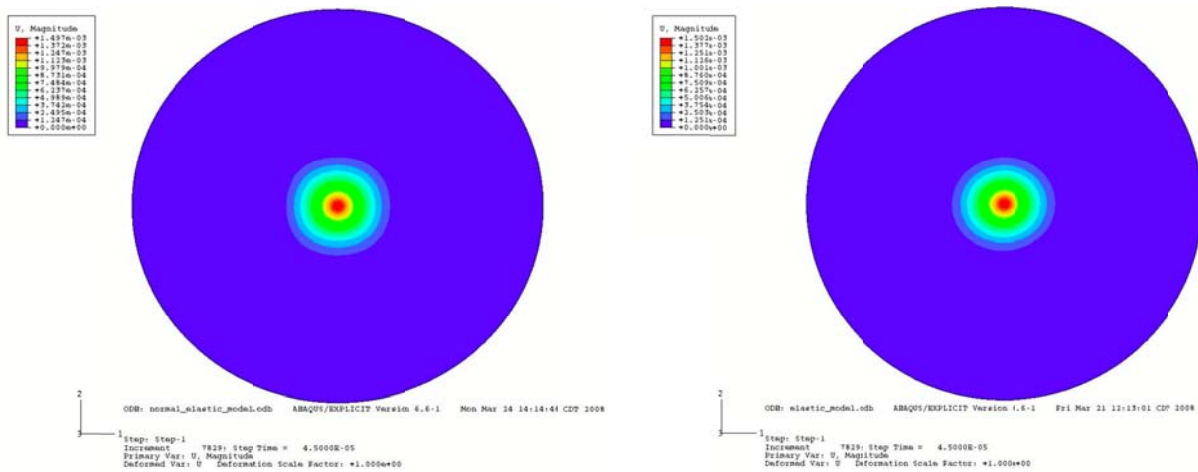
Figure 4. Deformation of the plate 45 µs after impact; left image: 0/90 plate and right image: helicoid
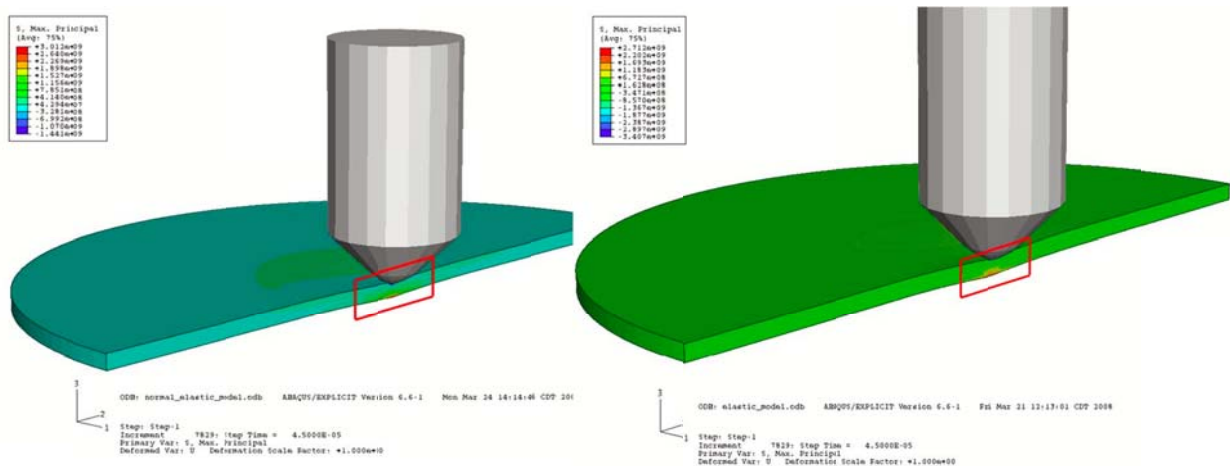
Figure 5. Stress contour of the plate 45 µs after impact; left image: 0/90 plate and right image: helicoid

10
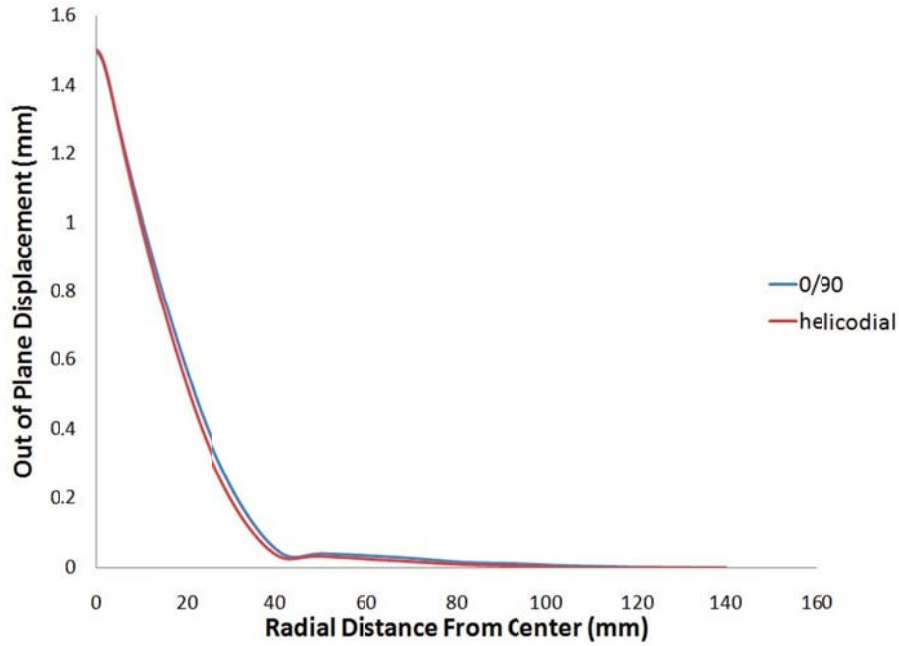
Figure 6. Out-of-plane displacement at 45 μs after impact for the 0/90 and helioidal plate.

Figure 6 shows displacement of the plate starting at the point of impact for both the 0/90 and helicoidal plates. The plot shows that the 0/90 and the helicoidal models have virtually identical through thickness displacements. The difference in the peak back side displacement between the two models is negligible. The peak stress differs by only about 10% Therefore, one does not expect significant differences in the dynamic or impact response of the 0/90 laminate and the helicoidal laminate in the early stages, when the elastic response is exhibited. Next, we consider the effect of delamination, by introducing a cohesive zone model.

3.1.2. Cohesive Zone Model for Delamination

A cohesive zone model was used in order to simulate delamination of the laminate under impact; this numerical implementation has 1,055,836 C3D8R elements, 353,496 COH3D8 elements, and 2,051,111 nodes. The elastic properties of the C3D8R elements are the same as those in the elastic model. However, each composite layer is connected to the next layer using a zero thickness layer
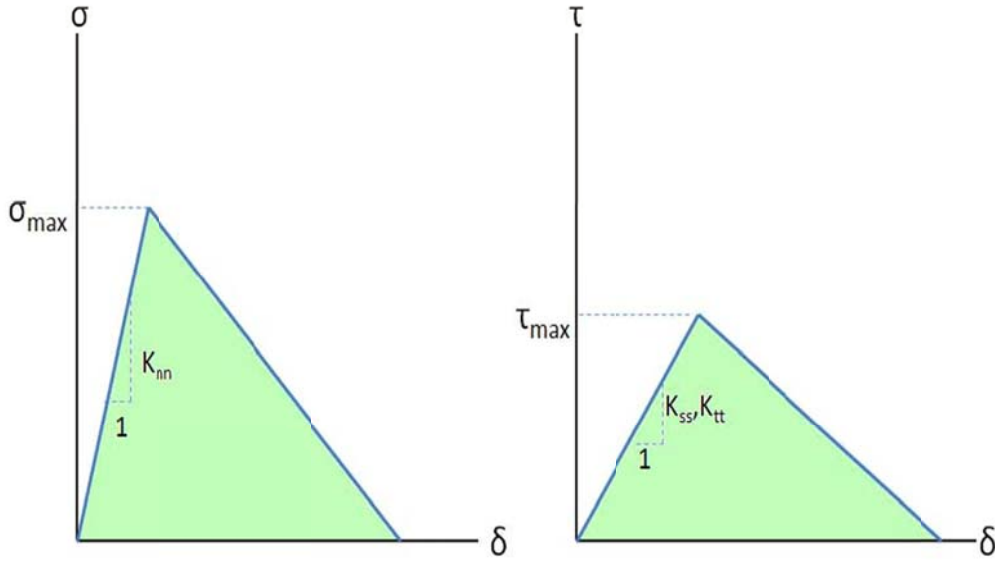
Figure 7. The peel (left) and shear (right) stress as a function of the separation (sliding) displacement.

of cohesive elements (COH3D8). Once the maximum normal stress or shear stress of a cohesive element is exceeded during impact the element stiffness will decay using the Benzeggagh-Kenane (BK) (1996) mixed mode failure criterion until the element is completely inactive. The BK criteria is useful when modeling materials where the fracture energies along the in-plane (first) and out-of-plane (second) shear directions are the same. The criterion is given by

$$G_n^c + \left(G_s^c - G_n^c \right) \frac{G_s + G_t}{G_n + G_s + G_t} = G^c$$

where the superscript c indicates fracture energy while subscripts n, s, and t are the normal, first shear, and second shear directions respectively. The pure peel and pure shear traction-separation laws are plotted in Figure 7. As shown in the figure, K_{nn}, and K_{ss}, K_{tt} are the uncoupled elastic modulus and two shear moduli. They define the slope on the first part of the stress vs. separation graphs. σ_{max} and τ_{max} are the highest stress values that can be reached before permanent material stiffness degradation is initiated. The shaded area under each graph is the uncoupled fracture energy $\left(G_n^c, G_s^c, G_t^c \right)$. The fracture energy can be calculated by dividing the square of the modal stress intensity factor k_i by the corresponding elastic modulus:

$$G_i = \frac{k_i^2}{K_{ii}}$$

Modeling with cohesive elements in this way allows a large displacement to effectively disconnect two layers of the composite material, thereby simulating a delamination. The cohesive element properties are given in Table 2. As with the elastic model in the previous simulation the results shown here correspond to a projectile velocity of 48.6 m/s

Table 2. Cohesive element properties

Property	K_{nn} (GPa)	K_{ss} (GPa)	K_{tt} (GPa)	σ_{max} (GPa)	τ_{max} (GPa)	G_n^c (GPa)	G_s^c (GPa)	G_t^c (GPa)
	4.5	1.7	1.7	10	8.6	55	100	100

As shown in Figure 8, the 1.68 GPa flexural strength of NCT304-1 Carbon Epoxy was not exceeded on the backside of plate in the 45.0 microsecond run time; this was also true for the helicoidal model. The maximum displacement this time was around 1.8 mm, reflecting the fact that the interlaminar properties make the specimen more compliant. The corresponding peak stress is about 1.24 GPa, significantly smaller than the elastic model. There is a small difference in the displacement through thickness between the helicoid and the 0/90, but this is not likely to be important.

Comparing the delamination zones in the two models shows a 16.6% increase in the number of debonded cohesive elements from the helicoidal model to the 0/90 model, suggesting that the helicoid could dissipate more energy. Comparing the simple elastic model to the cohesive model shows that delamination plays an important role in the deformation of a composite plate under dynamic loading conditions. At the center of impact the difference in displacement between the cohesive and elastic model was 0.36 mm for the 0/90 model. The difference in displacement for the helicoidal model was slightly less at 0.3 mm. By allowing plies to separate the plates are less stiff flexurally once a critical load has been reached. This decrease in flexural stiffness means there will be greater deflection in a delaminated plate than with an intact solid plate. However, including

delamination means that energy is absorbed by two mechanisms instead of simply by bending elastic material. For an armor to be effective it needs to be able to quickly disperse impact energy over a large area. The helicoidal layup more evenly distributes the impact energy across each layer than a 0/90. Therefore, the helicoidal plate should be able to absorb more energy through delamination than the 0/90 plate.

In order to understand the delamination areas seen in the helicoidal plates used in the high velocity experiments a corresponding simulation was created. This model uses the same element properties and geometry as the low speed cohesive model, but the projectile mass has been decreased to 13.5 grams and the velocity was increased to 200 m/s. In the physical experiments the projectile sheared through the first several layers of the plate; it was not possible to incorporate this type of material failure into the model. Therefore, the displacement results from the simulation will not match those seen in the laboratory. The simulation can provide insight into how delamination spreads through the layers that are not sheared.

Figure 9 shows the areas of delamination in the last nine cohesive layers of the model. The zone of separation in each layer is aligned to the fiber direction of the adjoining elastic elements. Therefore delamination is expected to be confined to a specific domain in each layer similar to that
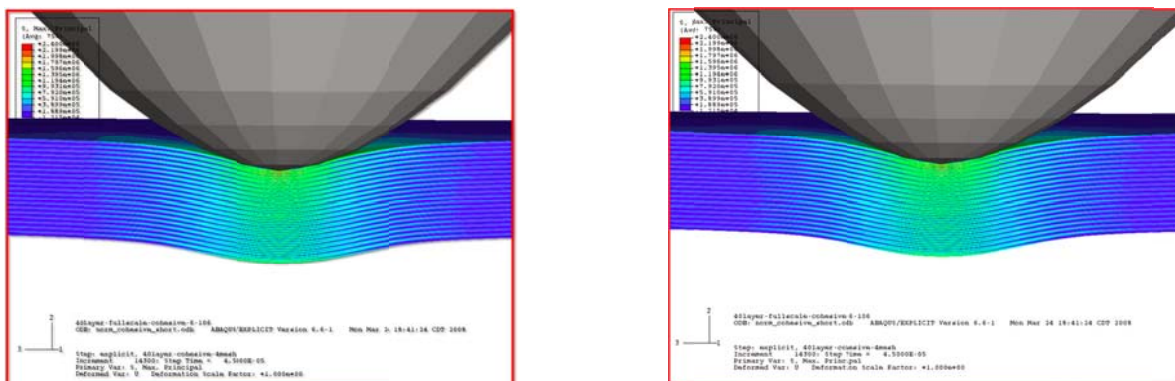
Figure 8. Deflection of the laminate (left: 0/90; right: helicoid) at 45 μs after impact.

shown in figure and not spread as easily as in the unidirectional or cross-ply laminates. This will provide a significant residual stiffness and strength to the composite.

3.1.3. Other Models

One of the early design concepts considered in this research used fiber layers which were to be subjected to tension during the curing phase of processing. This creates a prestress that would reduce the tendency for delamination. To simulate this in ABAQUS, the four 0° layers in the middle of the model were given an initial stress of 500 MPa (approximately 1/3 of the fiber's ultimate tensile stress). After reaching equilibrium with this initial condition, the model was impacted. Figure 10 shows a section of the plate after reaching equilibrium. The results showed a
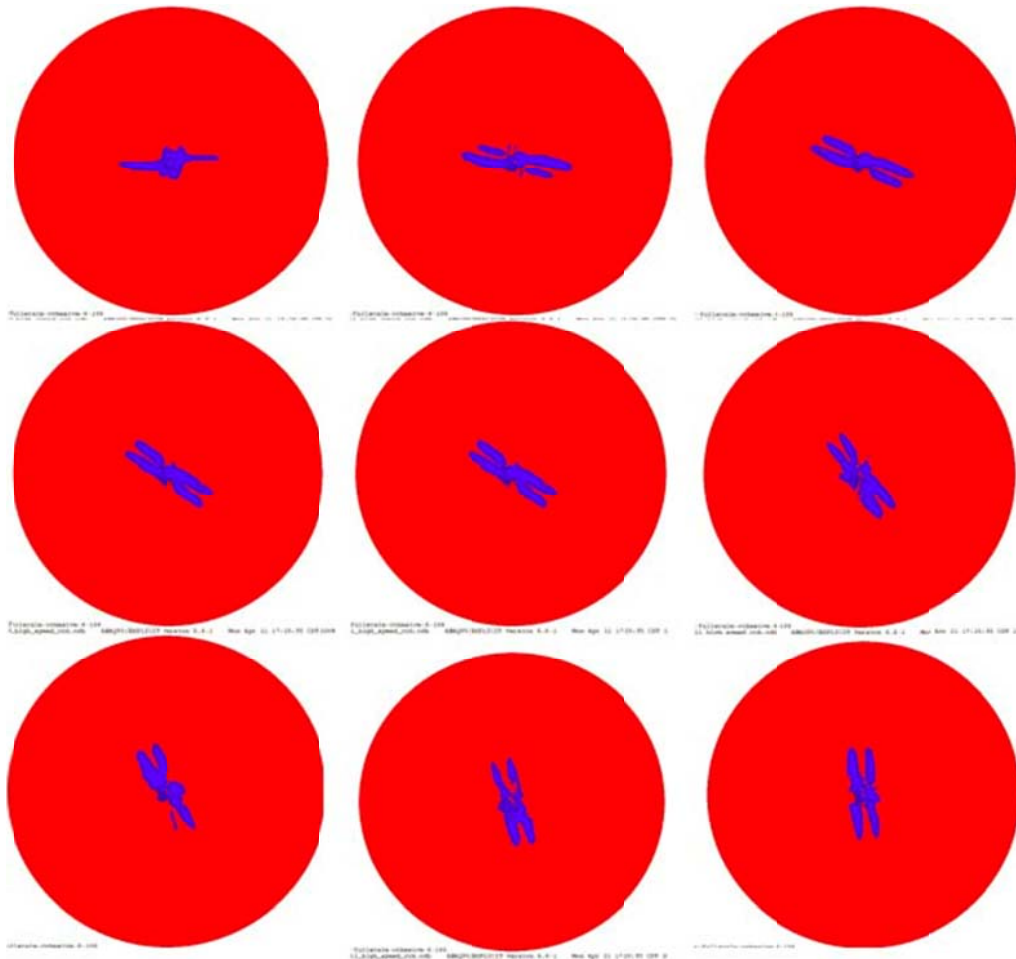
Figure 9. The delaminated region in the first nine interplay regions is shown by the blue shading.
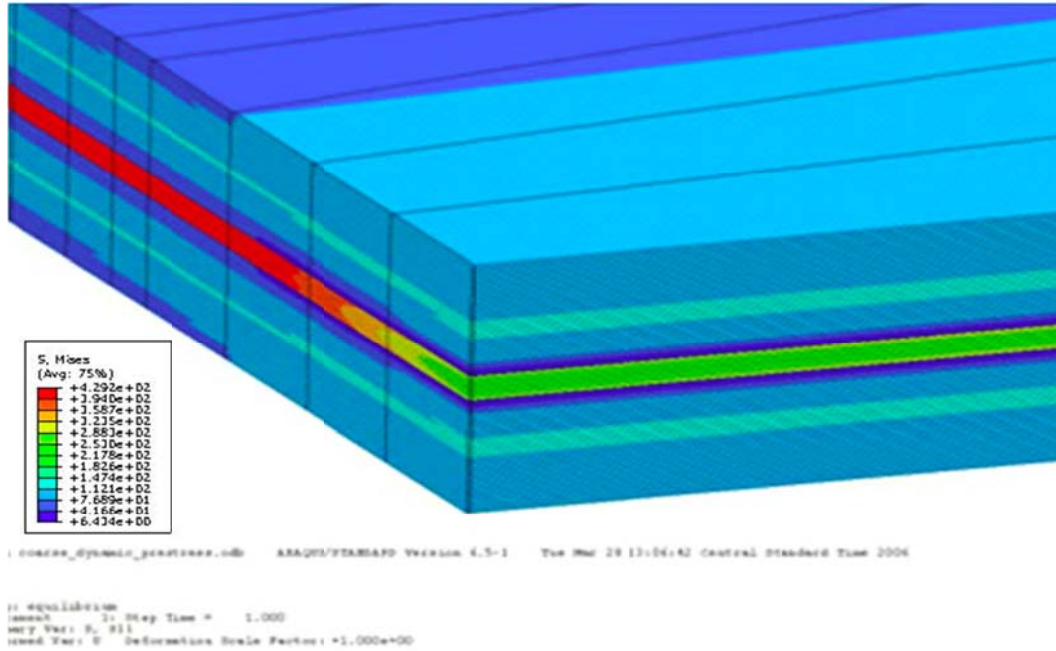
Figure 10. Distribution of residual stress caused by a 500 MPa tensile prestress in the middle four layers.

negligible decrease (less than 0.1%) in displacement on the backside of the model when prestress was included. Further investigation also revealed that the only method for manufacturing such a plate required a filament winding machine, which could only produce a fraction of the prestress used in the simulation; therefore, we did not pursue the prestress design further.

Another model that was experimented with used element deletion to model fiber breaks and matrix cracking. This model would deactivate any element that had exceeded its maximum allowable stress level. Incorporating this into the cohesive model resulted in solution times on the order of weeks even on high-end machines. Often the simulation would result in an uncoverged state. This type of analysis may be possible in the future with advances in processing power and finite element methods.

3.2. Experimental Investigation of the Impact Response of a Helicoidal Composites

Three different tests were performed: first, a quasi-static bending test was performed on a helicoidal sample. The purpose of this test was mainly to compare material properties with a previous study performed by Apicharthabrut and Ravi-Chandar (2006). The second test was designed to simulate the kinetic energy of a bullet impact by using a relatively low velocity, but massive projectile. This experiment gave some insight into the pre-fiber break failure of the plate; however complete penetration was not possible at such low velocities. It was therefore necessary to perform a third experiment where the composite plate was impacted with a small projectile traveling at a high velocity. Whenever possible, standard test methods and practices were employed. We describe these experiments in the following sections.

3.2.1. Quasi-Static Plate Bending Tests

Figure 11 shows the experimental set-up for quasi-static loading. The composite specimen is first clamped between two one-inch thick aluminum brackets. These brackets have a 10 inch diameter hole in the middle and are sandwiched around the composite plate using 16 periphery bolts. The clamped specimen is then placed under the crosshead of the Instron 4482 Universal Test Machine. A steel ball with a diameter of 0.5 inches is attached to the crosshead with a long steel bar. The crosshead is then lowered until the ball is in contact with the composite plate. In order
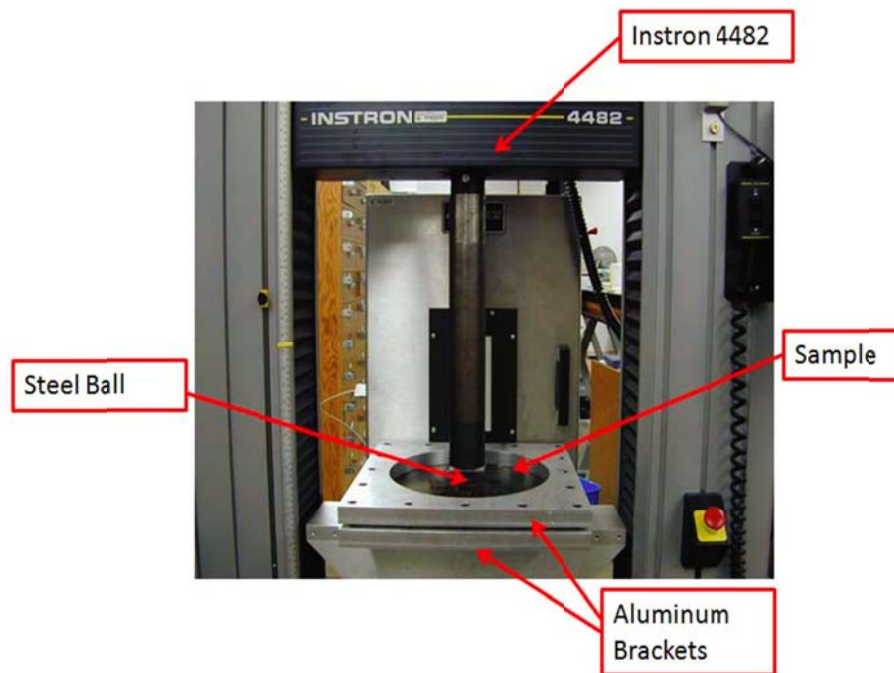
Figure 11. Plate bending test arrangement.
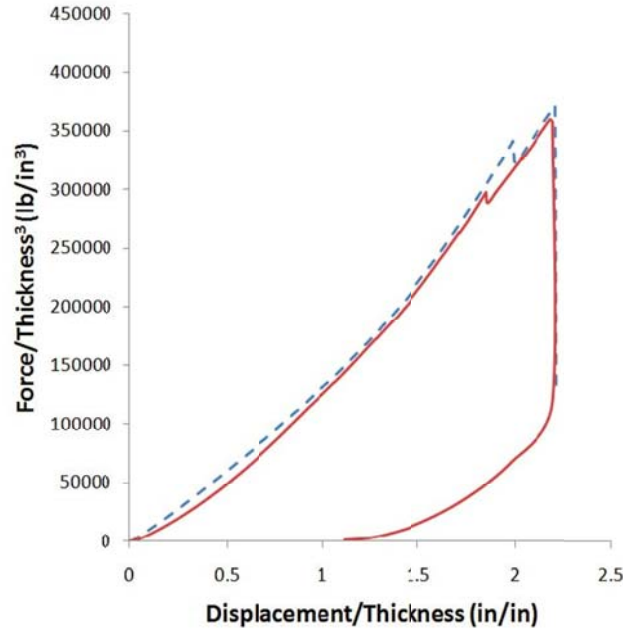
Figure 12. Load-defection response of clamped circular plate.

to achieve a quasi-static loading the crosshead is moved downward at a rate of 0.1 in/min. Material cracking can be heard throughout the experiment as the epoxy and the fibers break. Eventually, the plate fails completely and is not capable of supporting load anymore. The load-deflection response of the helicoidal composite is shown in Figure 12, with a comparison to the results of Apicharthabrut and Ravi-Chandar (2006); this should also be compared to the result shown in Figure 1. The newly fabricated plates exhibit a nearly identical response to bending as the earlier batch of helicoidal plates, and are significantly superior to the cross-ply laminates. Note that at the end of the test, the cross-ply exhibited a crack that breaks the plate into two pieces, while the helicoid exhibits localized cracking and hence a significant residual load carrying capability. The main objective of the present study is to examine whether this improved performance can be carried over to impact response. Two sets of experiments were performed: low-speed tests and high speed tests, but with nearly the same kinetic energy (about 750 J for the low speed and 460 J for the high speed impact tests).

 3.2.2. Low-Speed Impact Test

The first set of impact tests were performed on the carbon-fiber reinforced epoxy plates. The test
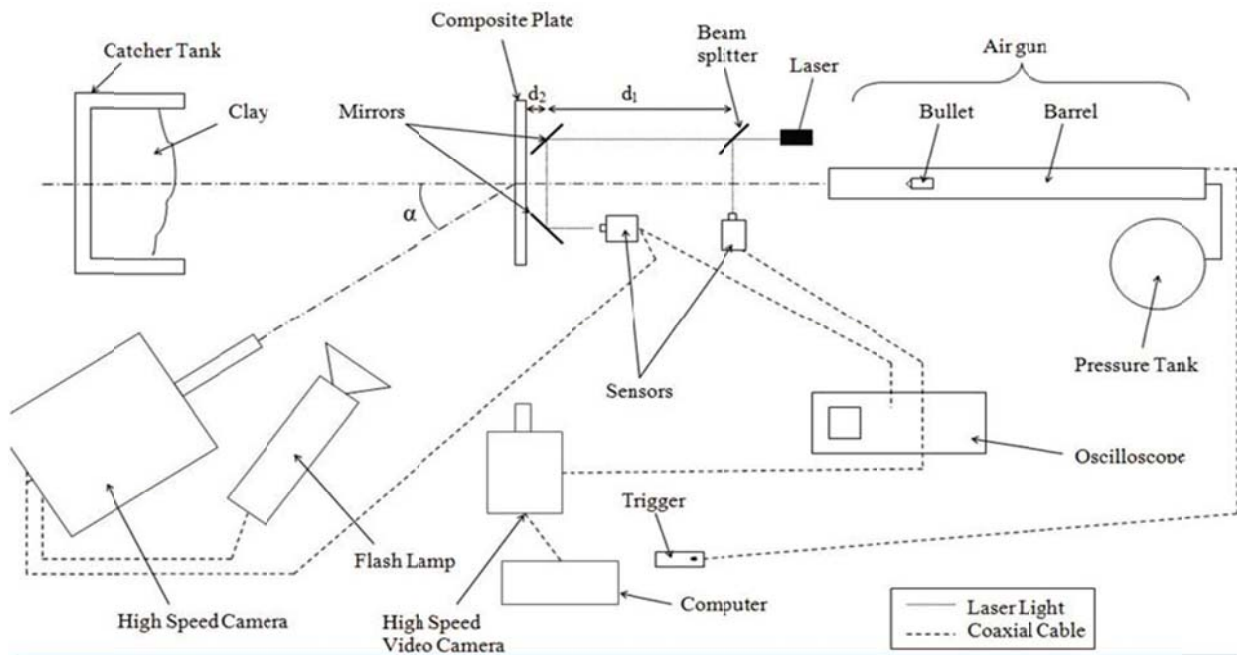
Figure 13. Test arrangement for low-speed impact tests on composite plates.

set-up is shown in Figure 13. Each test plate is placed between one inch thick aluminum plates as with the quasi-static bending tests described earlier. The test plate is then secured one meter from the end of the barrel of the gas gun. The plate is clamped to a solid frame which is then strapped to the floor with nylon cords. A laser beam crosses the path of the projectile at a distance of both one centimeter and ten centimeters from the plate. Light sensitive diodes are positioned to intercept the laser and generate a voltage pulse when the laser beam is broken by the projectile. Each pulse is recorded on an oscilloscope. A Cordin Model 550 high speed camera was used to record the response of the plate. The diode closest to the plate also triggers the high speed framing camera and its accompanying flash lamp. Likewise, the diode closest to the gun was used to trigger the high speed video camera that was used to monitor the overall impact phenomenon. Also along the path of the projectile, but behind the test plate, is a catcher tank filled with clay designed to stop the projectile, should the projectile completely penetrate the plate.

The out-of-plane displacement of the back surface of the specimen was monitored with the high speed camera. In order to make quantitative measurements, a grating method was used. A pattern of parallel lines spaced one mm apart was deposited on the specimen. The specimen was

Figure 14. Test arrangement for low-speed impact tests on composite plates.

then photographed at an angle to the plate normal; the projected length can then be used to extract the out-of-plane displacement of the specimen. On some of the early samples these lines were made from iron-on decals. Bonding the decals required the cured laminated to be placed in a hot press that was heated to 120 °F. The decal was then laid on top of the laminate, and then a thin rubber mat was placed on top of the decal. The press was lowered onto the mat, and a pressure of 100 psi was applied to it. The rubber mat helped to even out the pressure across the laminate; however, this method did not produce consistent results. The lines would often come out distorted or easily be separated from the plate. Later samples were taken to a professional screen printing company (www.actionscreengraphics.com). The silk screened lines are significantly more uniform than the iron-on decals. The paint thickness is less than 0.0254 mm and does not alter the response of the composite laminate. Figure 14 shows a finished plate, with lines printed on one side.

Before testing the out-of-plane displacement measuring procedure was calibrated. First, it is necessary to determine the angle, α, between the high speed image camera and the projectile's path. In order to determine α, a specimen with the line pattern is placed in the test location on a rotating stage, and a picture is then taken with the camera; next, the specimen rotated about the

vertical axis by an angle β and a second picture is taken. Image analysis software is used to measure the distance between the vertical lines before rotation L_1 and after rotation L_2. The angle α is then extracted by solving the following equation:

$$L_1 \cos\alpha = L_2 \cos(\alpha + \beta)$$

Triggering and timing proved to be very difficult with this experiment. Very few impacts were successfully recorded in this test due to complicated timing delays that were needed. Figure 15 shows all 30 frames captured by the high speed image camera during one impact event. In this experiment, the plate was impacted at 48.6 m/s with the 485 gram projectile. The capture rate on the camera was 30160 frames per second resulting in an interframe time of 33.2 μs. Impact occurs
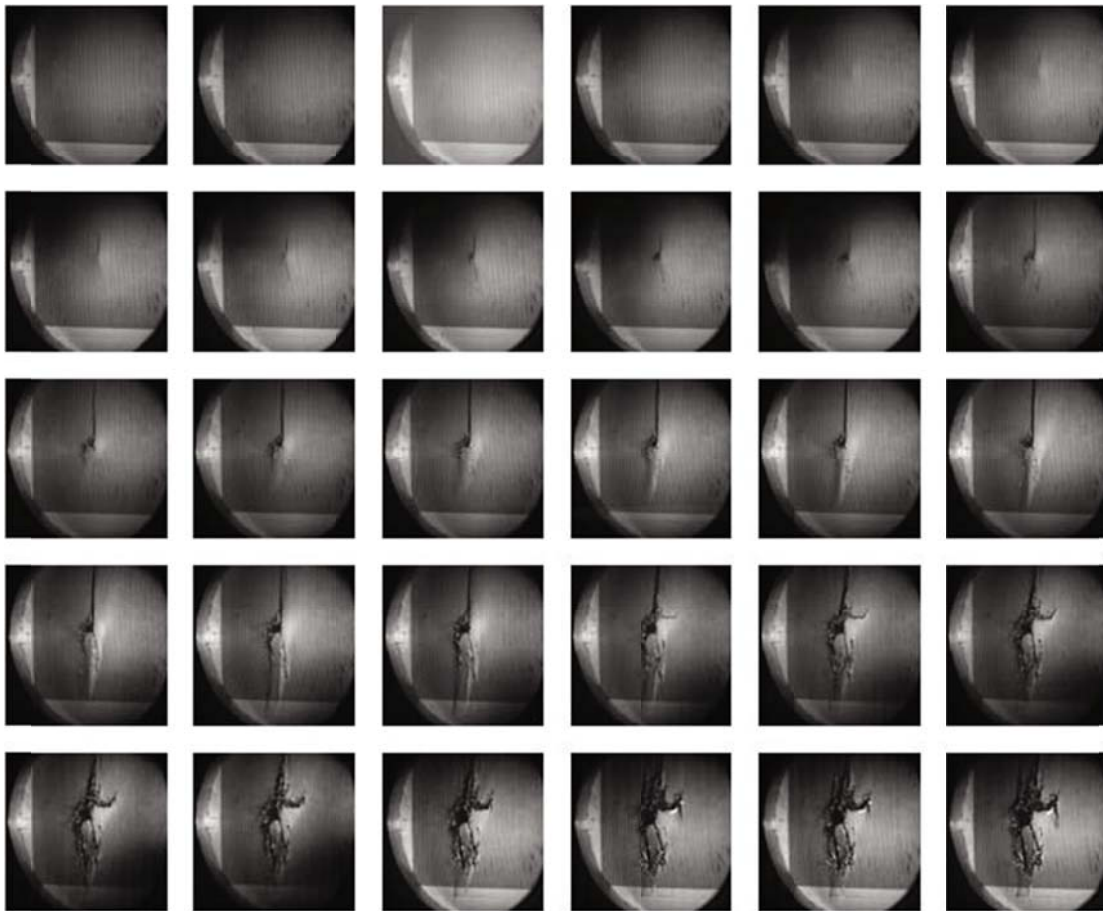

Figure 15. High speed images of the helicoidal plate under normal impact. Frames are 33.2 μs apart.

21

at a time between frames 4 and 5; these frames are shown enlarged in Figures 16. The printed lines in the figures are aligned to the 0° fiber direction.

The high speed images were processed to determine the out-of-plane displacement as indicated earlier. Figure 17a shows the variation of the out-of-plane displacement along a horizontal line, from the center towards the clamped boundary, at different times (frames 5 through 9). A comparison of these measurements to the results of the numerical simulation is shown in Figure 17b. Figure 18 shows a comparison of the overall deflection of the plate both from the experiment and the simulation. The maximum displacement at frame 8 was measured in the test to be 4.973 mm, between 99.5 and 132.6 microseconds after impact. The cohesive helicoidal model is used to calculate the deflection 121.5 microseconds after impact. The displacement prediction lies directly in the range observed in the physical experiment; the displacement profiles generated in both analyses match very closely as shown in Figure 17b. The model described in Section 3.1, with cohesive elements is capable of replicating the deflection response quite well. The first fiber break is apparent in frame 8; frames 7 and 8 are shown enlarged in Figure 19. Several fiber strands are apparent at the center of the plate in frame 8. While matrix cracking should precede fiber break, it is not possible to identify the formation of crack from these pictures. Figure 20 shows the progression of damage as the projectile continues to penetrate the plate. The final image captured with the high speed camera is shown in Figure 20b; the damage area is large, but complete penetration could not be achieved in the helicoidal composite.

With the demonstration that the ABAQUS model with cohesive elements is capable of replicating the overall deflection of the back surface, we explore the stress calculations. The peak backside stress at 121.5 microseconds after impact was calculated to be about 1.79 GPa. Comparing this to the tensile strength of the NCT403-1 carbon fiber of 1.68 GPa, one can infer that fiber break should occur at about this time; this is precisely what is observed at frame 8. The cohesive ABAQUS model can be considered valid up to the point where the stresses exceed the strength of the material. Since we do not have a good model for capturing fiber break, the simulations could not continue beyond this point.
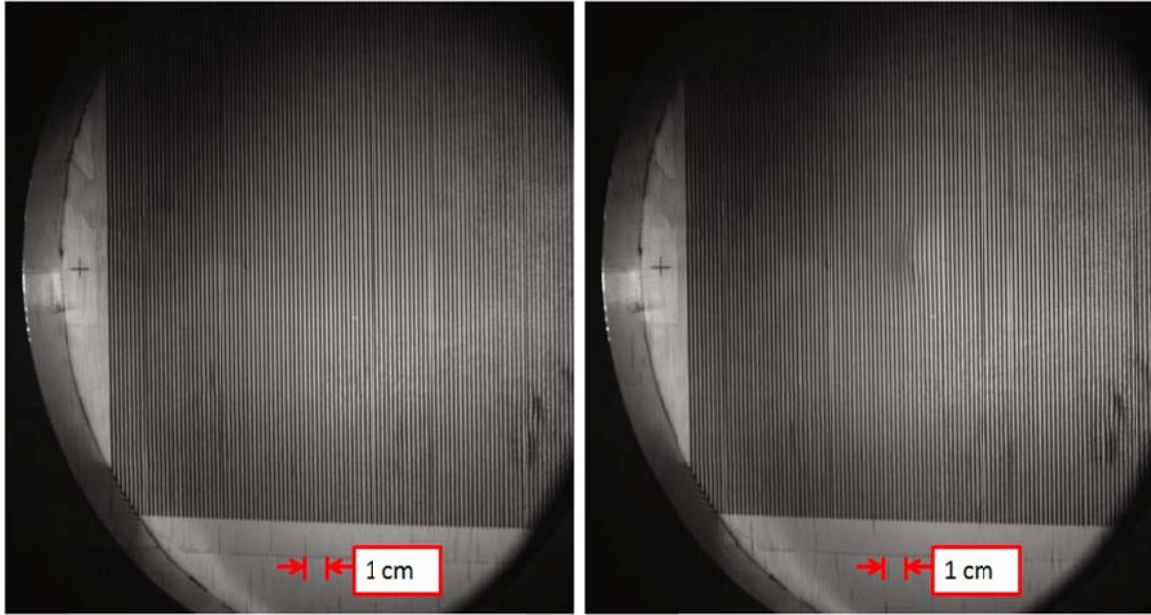
Figure 16. Enlarged view of frames 4 and 5 showing deflection behind the point of impact.
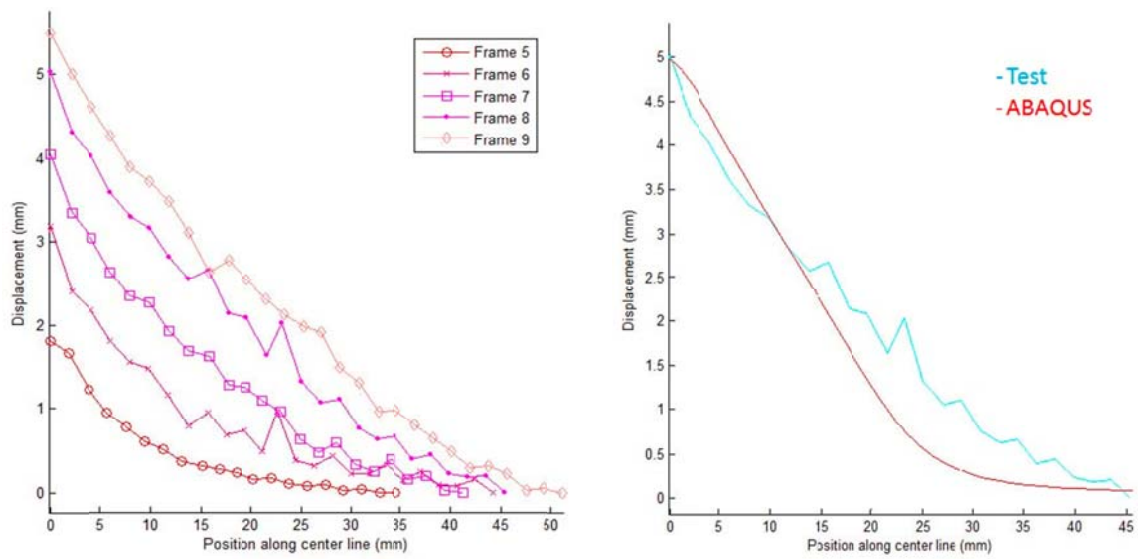
Figure 17. Load-defection response of clamped circular plate.
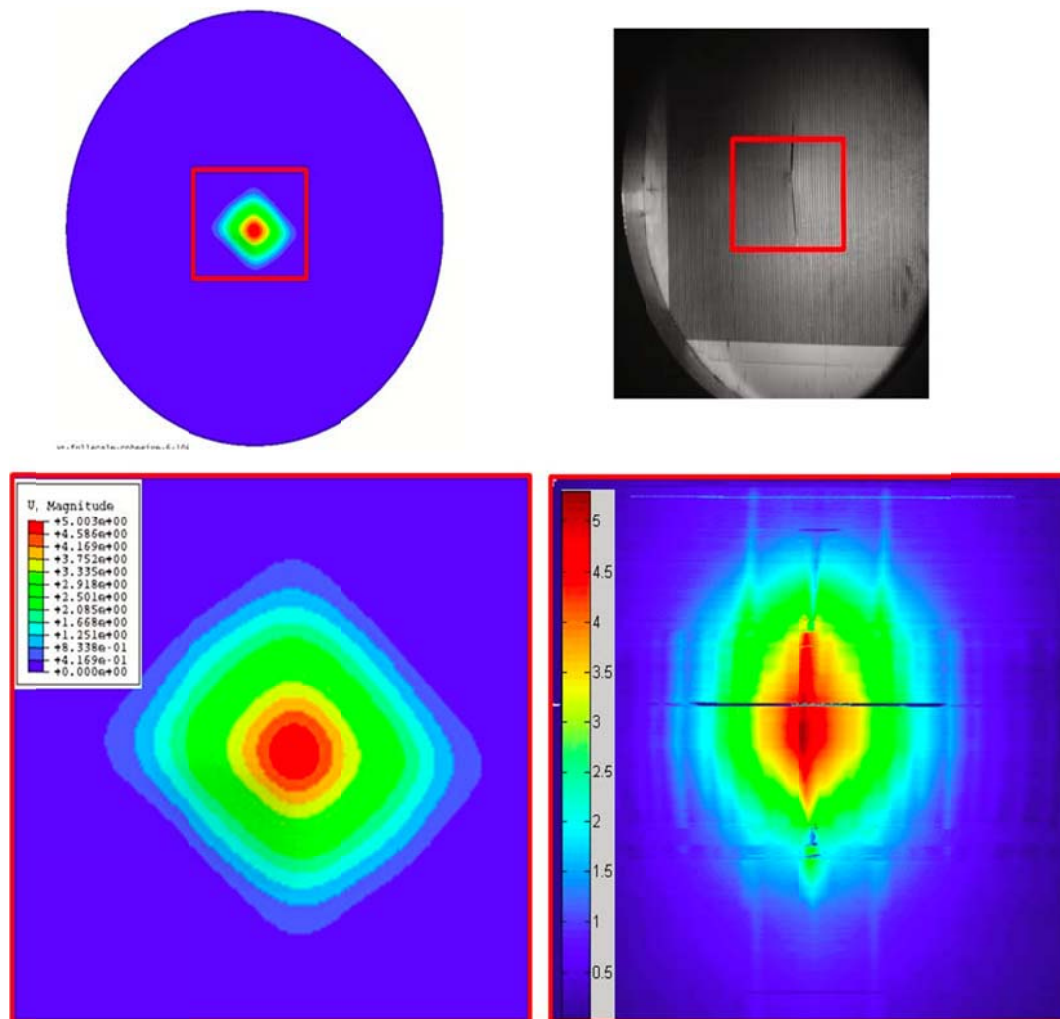
Figure 18. Load-defection response of clamped circular plate.
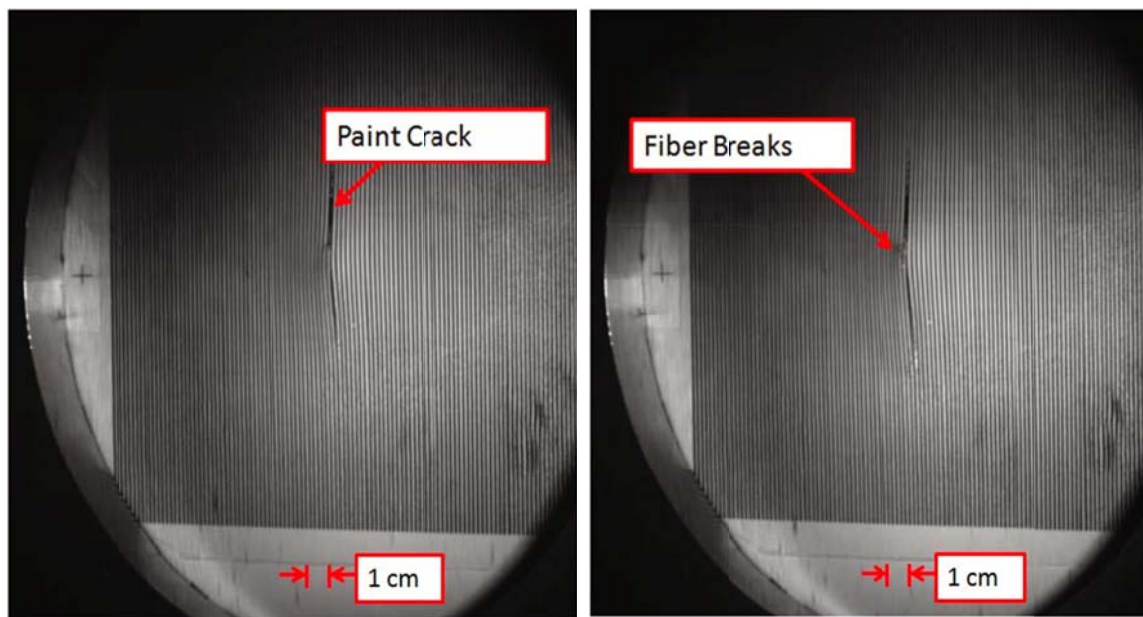
Figure 19. Enlarged view of frames 7 and 8 showing fiber break behind the point of impact.
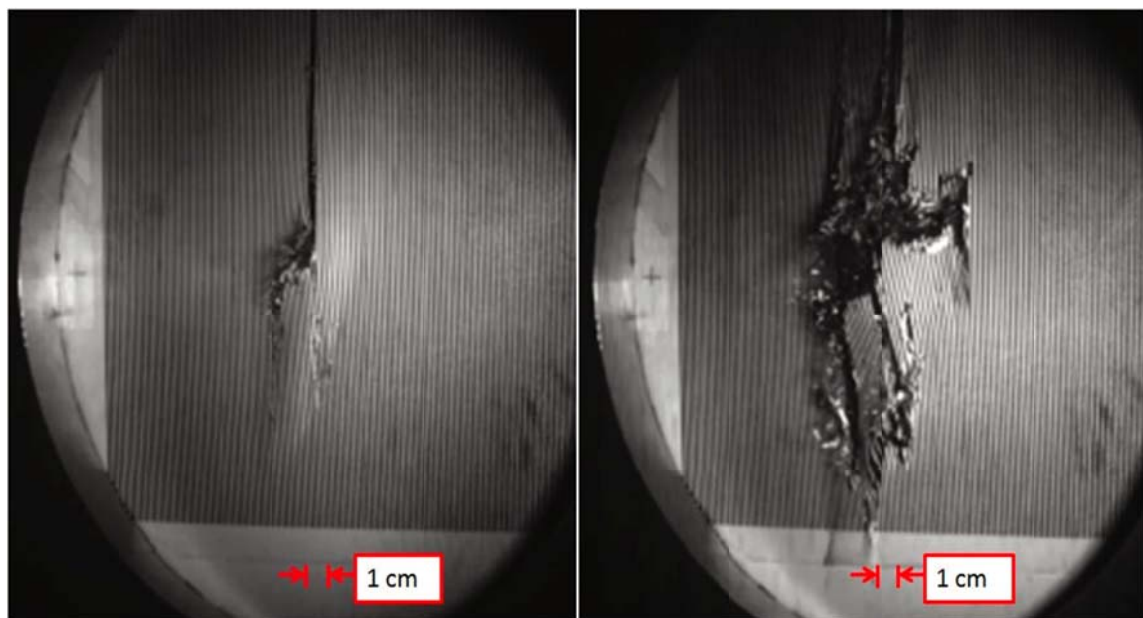
Figure 20. Enlarged view of frames 15 and 30 showing progression of failure behind the point of impact.

3.2.3. High-Speed Impact Tests

The optimal way to compare the ballistic effectiveness of different composite layups is to evaluate the amount of kinetic energy that each design can absorb during an impact event. This requires complete penetration by the projectile and measurements of pre and post impact velocity. The energy loss is usually given as a ballistic limit, defined as V_{50} and obtained from the following expression:

$$V_{50} = \sqrt{V_{in}^2 - V_{out}^2}$$

Or as the dynamic penetration energy, E_{dp}, defined as

$$E_{dp} = \frac{1}{2}m\left(V_{in}^2 - V_{out}^2\right)$$

The ballistic response of the composite plates was examined through experiments; six different groups of specimens were tested: (i) 0/90 cross-ply laminates of carbon fiber epoxy composite; (ii) helicoidal laminate of carbon-fiber epoxy composite; (iii) helicoidal laminate with staples for z-reinfrocement, of carbon-fiber epoxy composite; (iv) cross-ply laminate with polycarbonate interlayers for enhanced ductility and dissipation; (v) 0/45 alternating layers of plain-weave
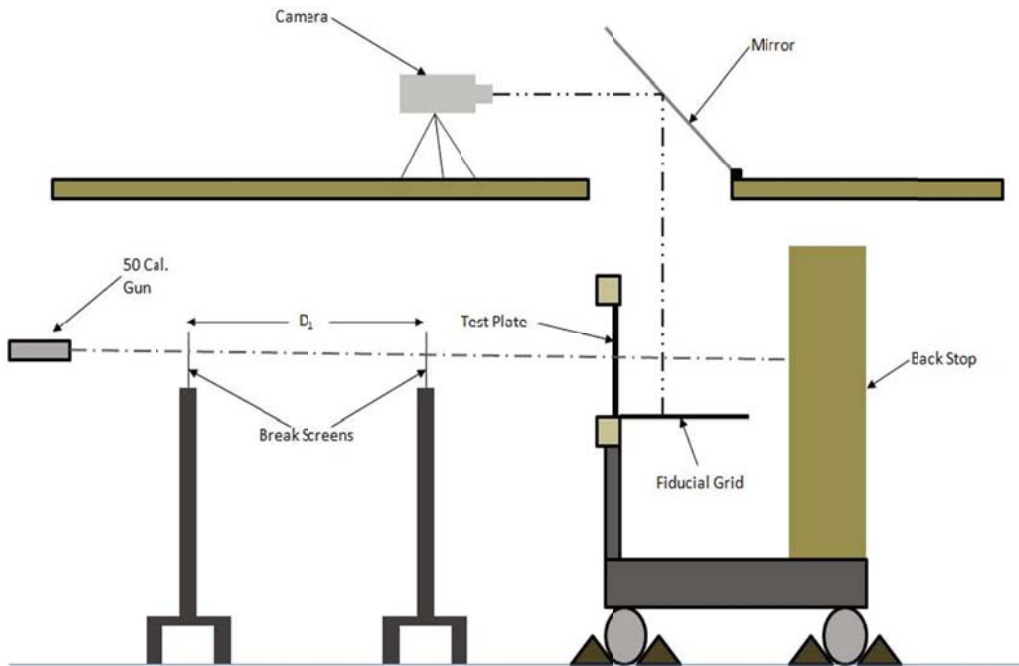
Figure 21.Schematic diagram of high speed impact test arrangement (elevation).
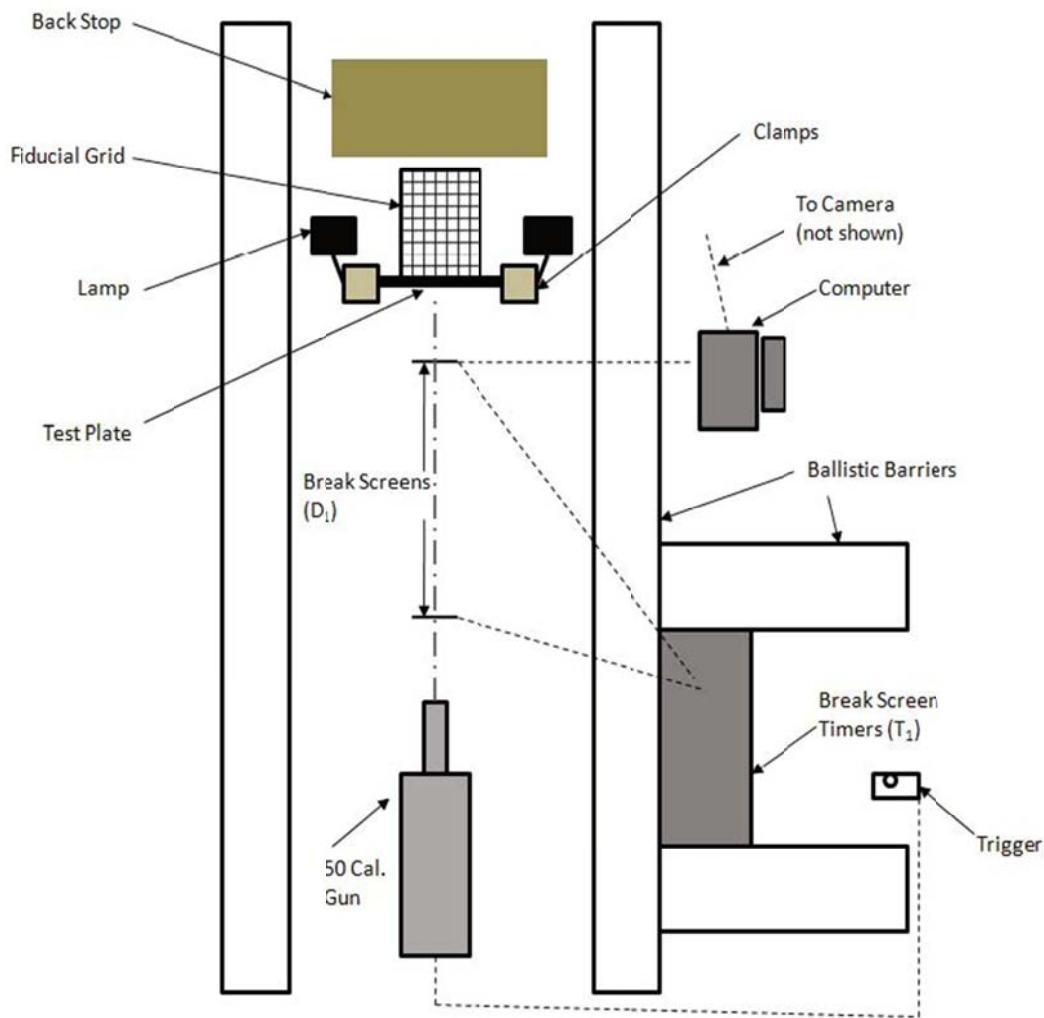
Figure 22. Schematic diagram of high speed impact test arrangement (plan view).

glass-fiber epoxy composite; (vi) plain-weave glass-fiber epoxy composite with helicoidal arrangement. All specimens were fabricated to have the same thickness of 6.8 mm.

The compressed gas gun setup described earlier was incapable of generating velocities for fully penetrating the plates; so the high velocity testing was done at The Institute for Advanced Technology (IAT), at The University of Texas at Austin. For this work a fixed 0.50 caliber rifle was used with varying amounts of gun powder to achieve the desired projectile speed. Figures 21 and 22 show the experimental arrangement used for the high velocity testing. Each test sample is sandwiched between two one- inch thick aluminum plates as discussed earlier for the bending tests. The aluminum plates have a 10 inch diameter hole in the center and are bolted together

around the sample. This grouping is then secured to a fixed platform in the firing range.

Two break screens are placed between the barrel of the gun and the test plate. These screens are fragile pieces of paper that have embedded wires that form an electrical circuit. When the projectile passes through the screens the current is broken and a timer and trigger signal are started or stopped. By having a known, fixed position for each break screen the pre-impact velocity, V_{in}, of the projectile can be determined. In order to determine the residual velocity after penetration, a grid with 5 mm line spacing is placed behind the specimen on a horizontal plane below the path of the projectile. Four 120 Watt halogen lights are positioned to illuminate the grid from multiple angles. A high speed video camera is placed above the firing range. The camera faces a mirror which angles the view across the back side of the sample and on to the grid. This camera is triggered by the second break screen. Recording at 19,047 frames per second, this camera captures images of the projectile once it has passed completely through the test plate. Since the number of pixels per meter in each image is known from initial calibration, the exit velocity, V_{out}, can be determined by counting the number of pixels the projectile moved in a set number of frames.

Because of safety concerns involved with live fire testing and the limited number of samples available, a strict testing procedure was necessary. The 0.50 caliber gun was aimed correctly by placing a laser in the barrel and adjusting both vertical and lateral placement. The laser must go through the center of both break screens and the sample. The sample as well as the break screens and the gun, were firmly secured in place. Each break screen and the high speed camera trigger was tested prior to each test to verify their proper operation.

The bullet used in this study is a 12.7 mm diameter fragment simulating projectile (FSP) as depicted in Figure 23. These highly standardized bullets are useful because they have sharp edges which can reproduce the cutting effects from shrapnel. The FSPs used in this study had a mass of 13.4 ± 0.1 grams. After weighing each FSP, a bullet casing is selected. These casings can be reused if a new priming cap is installed after each firing. Next, a small amount of gun powder is measured out. To achieve speeds between 170 – 250 m/s, only 1 to 2 grams of powder is needed. Because this is such a small amount of gun powder an even ignition is difficult to attain. The best results were accomplished with a black powder substitute instead of standard smokeless gun powder. After measuring the powder it was funneled into the casing, the powder was held in place with several pieces of wadding that was gently tapped down. With the wadding in position the FSP

Figure 23. Fragment simulating projectile.

is placed at the opening of the casing and the entire round is inserted into the chamber of the gun. Once the firing range is completely cleared and sealed off, the hammer is cocked back on the gun. A remote trigger was used to trip the hammer and fire the gun from a safe distance. The break screen data and video images were used to determine the input and exit velocities of the FSP; the specimen was recovered and examined for damage. Figure 24 shows a typical composite laminate that was subjected to four repeated impacts; the entry scar is significantly smaller than the exit scar. There is significant fiber break, delamination and overall failure in the last few layers than on the impact side. The details of the input and exit velocities of all tests performed on these specimens are given in Tables 3-8.

Figures 25-27 show the effect of single shot on carbon fiber epoxy plates plate. The 0/90, helicoid, and helicoid/staples each had two plates that were only shot a single time and two plates that were shot five times. The polycarbonate embedded carbon fiber laminate was shot six times at different locations on the plate. Figure 25a shows the impact side of a 0/90 laminate; the white circle marks the boundary of the delaminated area, identified by ultrasound. Figure 25b shows a section across the impact location, providing more detail of the delamination and fiber damage at
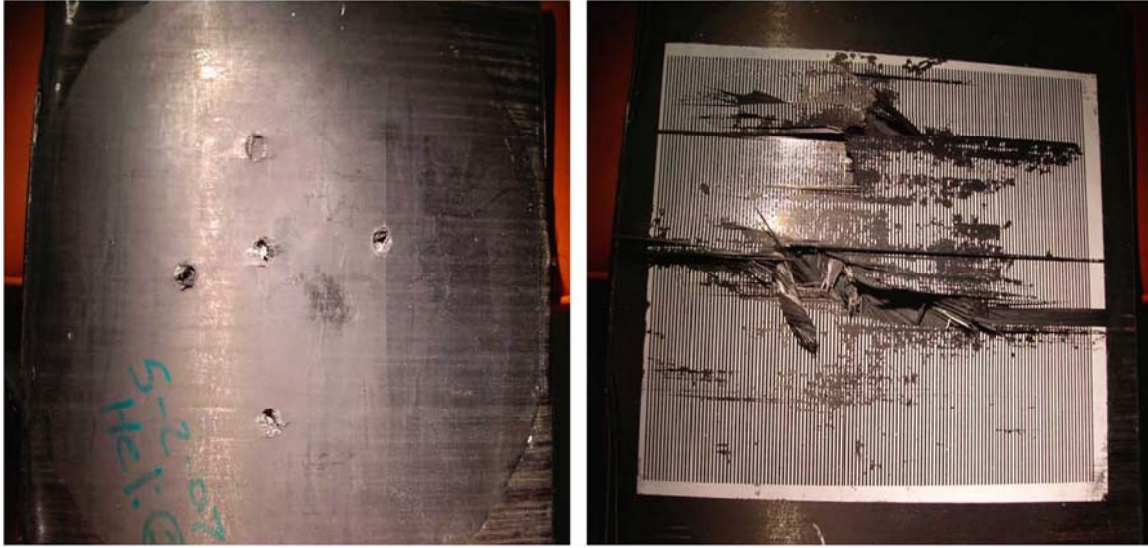
Figure 24. Post test images of the front and back sides of the 0/90 laminate.

the impact location; it is clear that every layer had delaminated. Figure 26a shows the impact side of a helicoidal laminate; the area of the delaminated zone appears to be 9 times larger than the 0/90 laminate. However, as can be seen in the cross-sectional image in Figure 26b, the delamination is isolated to a few layers with much of the thickness remaining intact. As indicated earlier in the simulation (Figure 9), the delamination is confined to a narrow region in each layer. When the laminate is reinforced in the z-direction with staples, there is very little delamination in the plate and damage is confined to the fibers in the vicinity of the impact (see Figure 27). Qualitatively, the failure mechanisms are again fiber break and delamination, with fiber break dominating the process at the high strain rates that arise in the high speed impact problem.

In an effort to determine the ballistic limit of the different types of laminates, the exit velocity is plotted as a function of the input velocity in Figures 28-31. From a curve fit to this data, one can deduce V_{50}. Figure 28 and Table 3 show the data and plot for the 0/90 cross-ply carbon-epoxy laminate. From a linear fit to the data, the ballistic limit is estimated to be $V_{50} = 142$ m/s; this is the baseline material property that will be used for comparison to the other laminates. Figure 29 and Table 4 show the data and plot for the helicoidal carbon-epoxy laminate; once again, a linear fit may be made to the data to extract V_{50}; the data for the 0/90 is shown for comparison. The ballistic limit is estimated to be $V_{50} = 176$ m/s, a nearly 25% improvement, but since the main

mechanism of energy dissipation appears to be the breakage of fibers, the architecture does not improve the overall performance significantly; as soon as the input velocity exceeds V_{50}, one cannot see any difference between the 0/90 and the helicoid. The corresponding results for the helicoid with staples are also shown in Figure 29 (and Table 5); the response is quite similar to that of the unreinforced helicoid. There might be a small increase in the ballistic limit, but once again as soon as this is exceeded, the penetration behavior appears to be unaltered. The woven glass fiber epoxy laminates exhibited very similar performance; the corresponding results are shown in Figure 30 and Tables 7 and 8. The data points fall almost exactly on that for the carbon fiber data suggesting that when the failure is fiber dominant, there is little difference between the carbon fibers and glass fibers. Finally, the laminates in which polycarbonate was interspersed between the carbon fiber layers exhibited improved performance; the corresponding results are shown in Figure 31 and Table 6. A systematic improvement in the performance is observed; the data are fitted by a logarithmic curve in Figure 31; the ballistic limit is estimated to be $V_{50} = 200$ m/s, a nearly 40% improvement; it is also clear that the entire ballistic response is shifted to larger impact levels. The underlying reason for this improvement in performance is the dynamic response of the polycarbonate. Polycarbonate is a ductile polymer, capable of significant shear deformation. Therefore, placing this material in between the carbon fiber lamina increases the shear resistance and increases the dissipation. Only one plate was manufactured with this material combination; additional experimentation is required in order to pursue this further and optimize the design.
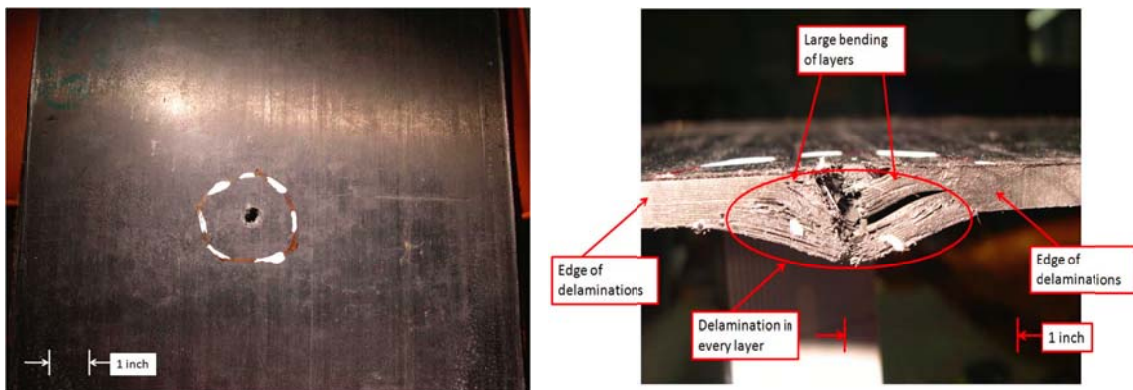
Figure 25. Post test images of the front side and cross section of the 0/90 laminate.

Figure 26. Post test images of the front side and cross section of the helicoidal laminate.
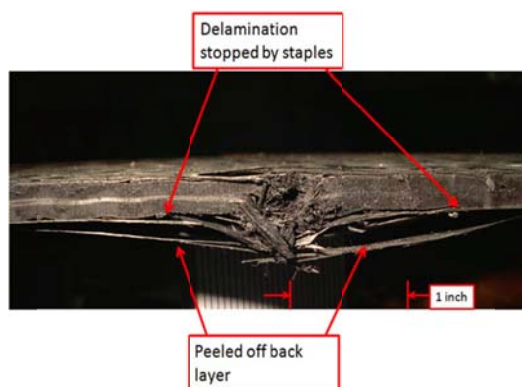
Figure 27. Post test images of the cross section of the helicoidal laminate with z-reinforcement.

Table 3: Cross-ply laminated plates; carbon-epoxy

Plate number	Architecture	Impact location	V_{in} (m/s)	V_{out} (m/s)	V_{50} (m/s)	Remarks
1	0/90	center	267	199	178	
2	0/90	center	203	105	174	
2	0/90	above center	132	0	132	incomplete penetration
2	0/90	right of center	169	0	169	projectile embedded
2	0/90	left of center	191	92	167	
2	0/90	below center	192	96	167	
3	0/90	center	240	174	165	
3	0/90	top	227	154	167	
3	0/90	right of center	245	174	172	
3	0/90	bottom	227	157	164	
3	0/90	left of center	229	152	171	
4	0/90	center	233	160	169	

Table 4: Helicoidal plates without z-reinforcement; carbon-epoxy

Plate number	Architecture	Impact location	V_{in} (m/s)	V_{out} (m/s)	V_{50} (m/s)	Remarks
6	Helicoid	center	231	143	181	
7	Helicoid	center	239	139	195	
7	Helicoid	below center	244	151	191	
7	Helicoid	above center	174	0	174	incomplete penetration
7	Helicoid	right of center	235	146	184	
7	Helicoid	left of center	215	125	175	
12	Helicoid	center	223	132	179	
14	Helicoid	top	217	106	189	
14	Helicoid	left of center	258	193	171	
14	Helicoid	bottom	215	93	194	
14	Helicoid	right of center	224	79	210	

Table 5: Helicoidal plates with z-reinforcement staples; carbon-epoxy

Plate number	Architecture	Impact location	V_{in} (m/s)	V_{out} (m/s)	V_{50} (m/s)	Remarks
15	Staple/Helicoid	center	250	174	180	
16	Staple/Helicoid	center	287	221	184	
17	Staple/Helicoid	center	226	134	182	
17	Staple/Helicoid	top	202	100	176	
17	Staple/Helicoid	right of center	197	0	197	incomplete penetration
17	Staple/Helicoid	bottom	221	136	175	
17	Staple/Helicoid	left of center	249	175	176	
18	Staple/Helicoid	center	185	0	185	incomplete penetration
18	Staple/Helicoid	above center	189	17	188	
18	Staple/Helicoid	below center	176	0	176	incomplete penetration
18	Staple/Helicoid	left of center	183	0	183	incomplete penetration
18	Staple/Helicoid	right of center	171	0	171	incomplete penetration

Table 6: Helicoidal plates with polymer layers; carbon-epoxy

Plate number	Architecture	Impact location	V_{in} (m/s)	V_{out} (m/s)	V_{50} (m/s)	Remarks
22	polycarbonate	center	205	10	205	
22	polycarbonate	top	210	37	207	
22	polycarbonate	right of center	218	0	218	incomplete penetration
22	polycarbonate	left of center	230	56	223	
22	polycarbonate	bottom	205	0	205	incomplete penetration
22	polycarbonate	corner	263	86	249	

Table 7: Cross-ply plates; glass-epoxy

Plate number	Architecture	V_{in} (m/s)	V_{out} (m/s)	V_{50} (m/s)
1	Uni-1-Shot-001	313	261	173
2	Uni-2-Shot-001	286	238	160
2	Uni-2-Shot-002	283	226	171
2	Uni-2-Shot-003	258	194	170
3	Cross-1-Shot-001	259	202	162
3	Cross-1-Shot-002	283	226	170
3	Cross-1-Shot-003	267	218	153
4	Cross-2-Shot-001	220	161	150

Table 8: Helicoidal plates; glass-epoxy

Plate number	Architecture	V_{in} (m/s)	V_{out} (m/s)	V_{50} (m/s)
5	Helicoid-1-Shoot-001	281	234	156
5	Helicoid-1-Shoot-002	261	199	168
5	Helicoid-1-Shoot-003	262	205	164
6	Helicoid-2-Shoot-001	237	174	161
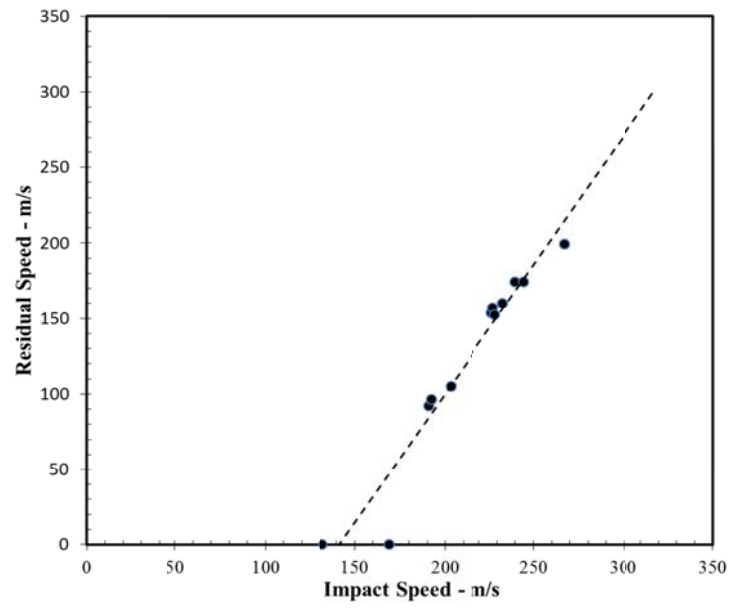
Figure 28. Residual velocity as a function of the impact velocity; 0/90 cross-ply
laminate of carbon epoxy.

Figure 29. Residual velocity as a function of the impact velocity; helicoidal
laminate of carbon epoxy without and with z-reinfrocement.

Figure 30. Residual velocity as a function of the impact velocity; cross-ply and helicoidal glass fiber – epoxy laminate.
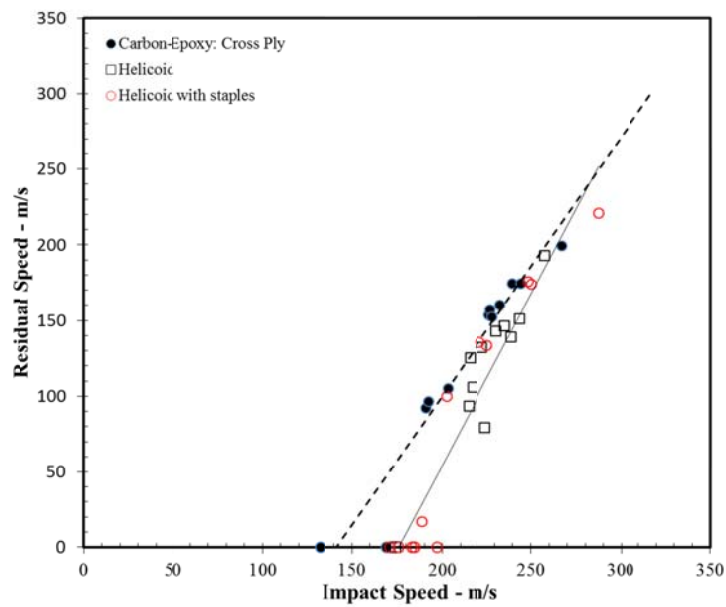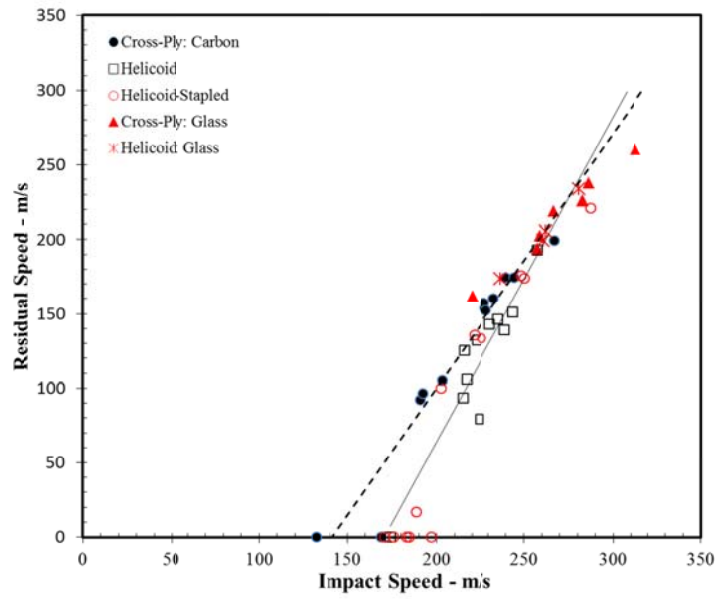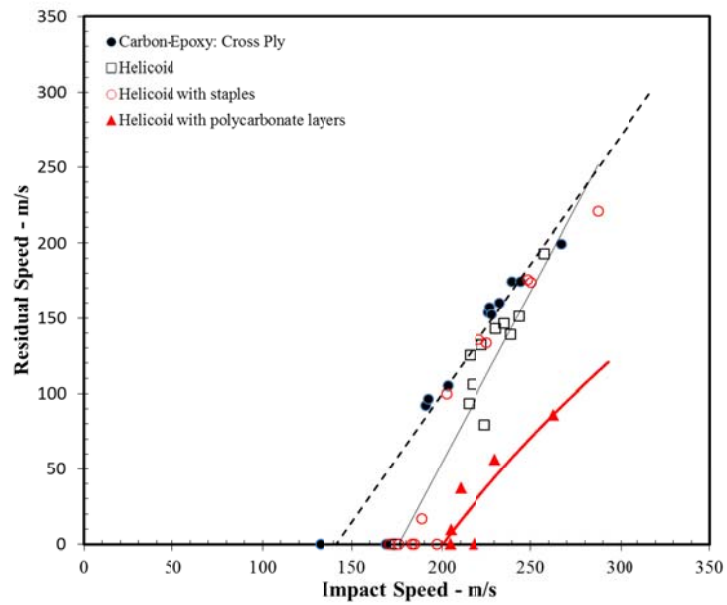

Figure 31. Residual velocity as a function of the impact velocity; 0/90 cross-ply laminate of carbon epoxy with alternating layers of polycarbonate film.

4. Summary and Conclusions

The purpose of this research was to experiment with unconventional layups in composite laminates and to improve on the ballistic impact performance of conventional composites. Because one of the primary failure modes of composite materials is delamination, several designs were created that attempt to minimize the interlaminar stresses that cause delamination. These designs include a helicoidal layup [0/10/20/30/40/50/60/70/80/90/100/110/120/130/140/150/160/170/(0)$_2$]$_s$, a helicoidal layup with through thickness support provided by stainless steel staples, a plain-weave glass-fiber with 0/45 as well as helicoidal arrangement, and a [(0/plastic/90/plastic)6/0/plastic/(0/plastic/90/plastic)6/0] layups (with polycarbonate as the plastic material). These designs were compared to a standard [(0/90)19/0]$_s$ layup.

Three separate experiments were performed on the composite plates. The first one, under quasi-static loading, indicated that a helicoidal plate would take significantly more load before failure than a standard orthogonal layup. The second set of tests performed was a low speed dynamic impact analysis. The plates were impacted with a low velocity (but massive) projectile. This allowed displacement measurements to be taken on the backside of the plate by a high speed camera. Analysis was conducted using the ABAQUS finite element software. Each lamina was discretized in the simulation and the helicoidal and 0/90 layups were compared under different loading conditions. A cohesive zone model was used to capture the delamination behavior of the laminate. The results showed that the helicoidal model was less prone to delamination during an impact event. In the final set of experiments each plate was penetrated multiple times by a fragment simulating projectile. By measuring the velocity of the projectile before and after impact, it was possible to determine how much energy was absorbed by each of the different layups. The helicoidal and helicoidal with staples both performed slightly better than the standard 0/90 design in terms of the ballistic limit V_{50}. The stapled design retained much of its strength after the first shot; the The design with polycarbonate layers absorbed considerably more energy than any of the other designs and exhibited a 40% increase in V_{50}.

Each composite design studied in this research has its own unique failure mode. The standard 0/90 layup delaminated in nearly every layer; however, the delamination was confined to a region within a one inch radius of the impact. The helicoidal design had a long thin line of delamination in

most layers. The area of delamination extended more three inches from the point impact along the fiber direction, but was less than a half inch wide. The stapled helicoidal design had the least amount of delamination. Instead of bending the plate and forcing the layers to separate, the projectile sheared its way through the fibers and plugged out material. The staples prevented any damage accumulation from happening after the first shot. The one mode of failure that all the plates shared was shearing of the fibers in the first several layers. The FSP round has two sharp edges that allow it to slice through material as it penetrates. The composite plate that had layers of polycarbonate proved to have the highest ballistic limit. Experimenting with other materials such as glass fiber, ceramics, and high temperature resistant plastics may show even better results.

REFERENCES

T. Apicharttabrut, and K. Ravi-Chandar, 2006, Impact response of helicoidal composites, *Mechanics of Advanced Materials and Structures*, **13**, 61-76.

Y.A. Bahei-El-Din, M.A. Zikry, A.M. Rajendran, 2003, Impact-induced deformation fields in 3D cellular woven composites, *Composites: Part A*, **34**, 765–778.

J.N. Baucom and M.A. Zikry, 2003, Evolution of failure mechanisms in 2D and 3D woven composite systems under quasi-static perforation, *Journal of Composite Materials*, 37, 1651-1674.

H. Chai, C.D. Babcock and W.G. Knauss, 1981, One dimensional modelling of failure in laminated plates by delamination buckling, *International Journal of Solids and Structures,* **17,,** 1069-1083.

H. Chai, W.G. Knauss and C.D. Babcock, 1983, Observation of damage growth in compressively loaded laminates," Experimental Mechanics, 23, 329-337.

L. Cheng, A. Thomas, J.L. Glancey and A.M. Karlssson, 2011, Mechanical behavior of bio-inspired laminated composites, **Composites A**, **42**, 211-220.

R.M. Christensen and S.J. DeTeresa, 1992, Elimination/minimization of edge-induced stress singularities in fiber composite laminates, *International Journal of Solids and Structures,* **29,** 1221-1231.

B.N. Cox K.L. Rugg and R. Massabo, 2002, Mixed mode delamination of polymer composite laminates reinforced through the thickness by z-fibers, *Journal of Composites Part A*, **33**, 177–190, 2002.

H.M. Hsiao, I.M. Daniel and R.D. Cordes, 1998, Dynamic compressive behavior of thick composite materials. *Experimental Mechanics*, **38**, 172-180.

T. Jianxin and C.T. Sun, 1998, Influence of ply orientation on delamination in composite laminates, *Journal of Composite Materials*, **32**, 1933–1947.

M. Kenane M.L. Benzeggagh, 1996, Measurement of mixed-mode delamination fracture toughness of unidirectional glass/epoxy composites with mixed-mode bending apparatus. *Compos. Sci. Technol,* **49**:439449.

W.J. Liou, 1997, Impact analysis of laminated composite plates with statical indentation laws, *Journal of Computers and Structures*, **62**, 817-829.

A.C. Neville, 1993, Biology of fibrous composites: development beyond the cell membrane, Cambridge University Press.

N.J. Pagano, 1978, Free edge stress fields in composite laminates, *International Journal of Solids and Structures,* **14,,** 401-406.

K.L. Rugg, B.N. Cox, K.E. Ward and G.O. Sherrick, 1998, Damage mechanisms for angled through-thickness rod reinforcement in carbon-epoxy laminates, *Composites Part A*, **29A**, 1603-1613.

K.L. Rugg, B.N. Cox and R. Massabo, 2002, Mixed mode delamination of polymer composite laminates reinforced through the thickness by z-fibers, *Composites Part A*, **33**, 177-190.

A.P. Suvorov and G.J. Dvorak, 2001a, Optimized fiber prestress for reduction of free-edge stresses in composite laminates, *Internatinal Journal of Solids and Structures*, **38**, 6751-6786.

A.P. Suvorov and G.J. Dvorak, 2001b, Optimal design of prestressed laminate/ceramic plate assemblies, *Meccanica*, **36**, 37-109.

J. Tao and C.T. Sun, 1998, Influence of ply orientation on delamination in composite laminates, *Journal of Composite Materials*, **32**, 1933-1947.

Appendix A. Design of the helicoidal architecture

Since the design parameter space – of material properties, property gradation, residual and pre-stress etc – is quite large, we approached the design from a geometric perspective. Considering only a plate structure, limiting the thickness to a nominal 0.25 in, and using standard prepregs, the starting parameters of the design of the helicoids were well constrained. Limiting the plate thickness to 0.25 *in* enabled experimental comparison to other graphite-epoxy plates of classical lamination architectures. Within these constraints, we have potentially 40 layers to distribute across the plate thickness. Taking a cue from biological composites, if we use an orientation change of 10° between neighboring layers, two pitches of a helix can be described in 36 layers. The additional 4 layers were placed in middle, all oriented in the 0° direction; in applications, this may be taken as the direction of the most common loading. In order to eliminate or minimize the elastic coupling between extension, bending and twisting deformations, we attempted to enforce symmetry and balance of the lamination about the middle plane of the plate. Both symmetry and balance can be accommodated by using the following graded architecture for the lamination sequence: $[180/170/160/150/140/130/120/110/100/90/80/70/60/50/40/30/20/10/(0)2]_s$. This gradation in the orientation of the fibers in the helicoidal composite is shown in Figure A-1.
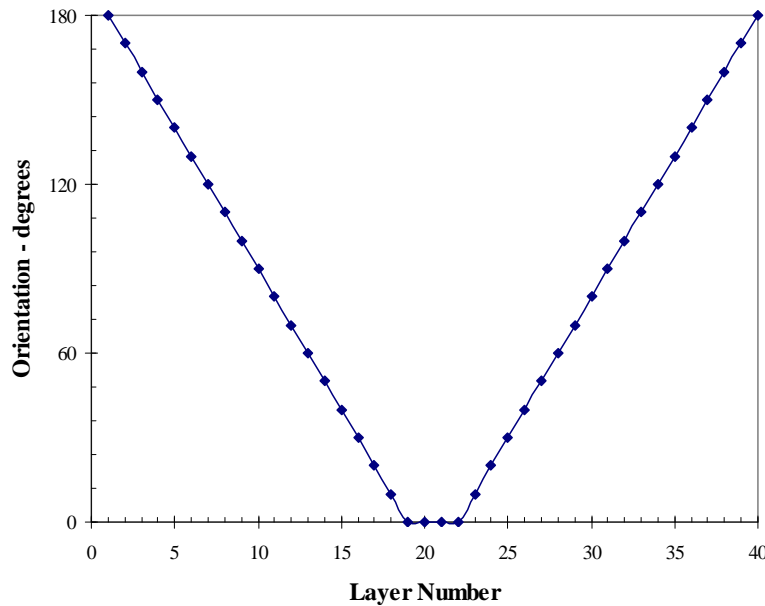

Figure A-1. Orientation of the layers of the helicoidal composite.

Clearly, there are many other possible options for the lamination, and an optimization of the orientation needs to be evaluated. It is also possible to consider specific layups for each particular application. This was not addressed in the current research program.

The pre-pregs are carbon-epoxy rolls obtained from Newport Adhesives and Composites (designation NCT 304-1). The nominal properties of this material are listed in Table A-1. The properties of the prepregs assumed in our analysis are given below:

$$E_1 = 124\,\text{GPa}, E_2 = 12.5\,\text{GPa}, G_{12} = 4.4\,\text{GPa}, \nu_{12} = 0.303, \nu_{21} = 0.03$$

For the 40 layer lamination described above, the laminate stiffness matrix is easily calculated and is shown below:

$$\mathbf{A} = \begin{bmatrix} 493 & 116 & 0 \\ 116 & 359 & 0 \\ 0 & 0 & 121 \end{bmatrix} \times 10^6 \,\text{N/m}\,; \ \mathbf{B} = [0]\,; \ \mathbf{D} = \begin{bmatrix} 2000 & 419 & -424 \\ 491 & 1370 & -259 \\ -424 & -259 & 512 \end{bmatrix} \text{N/m}$$

The fact that all components of the **B** matrix are zero could have been guessed from the symmetry of the lamination. Also, since the lamination is balanced, the A_{16}, A_{26} terms are also identically zero. Since there are no cross-ply arrangements, the D_{16} and D_{26} terms do not disappear and hence there is an elastic coupling between bending and twisting. One may also calculate the effective engineering constants of the laminate; these are found to be

$$E_x = 56.4\,\text{GPa}, E_y = 46.1\,\text{GPa}, G_{xy} = 17.0\,\text{GPa}, \nu_{xy} = 0.324, \nu_{yx} = 0.265$$

As can be determined from these engineering constants, the gradual change in the properties of the neighboring layers results in a nearly isotropic response of the laminate. To exhibit this more clearly, the variation of the engineering stiffness of the laminate as a function of the orientation with respect to the global x-direction (the direction with four layers of zeros in the middle section) is shown in Figure A-2. The C_{11} and C_{22} stiffness components vary very little as a function of the orientation; it is also important to observe that the C_{16}, C_{26} stiffnesses are small, suggesting that the coupling of extension to shear is small, but nonzero. If the extra layers of 0° in the middle of the plate are removed, a perfectly isotropic structure can be obtained; however, that is not the main objective of the helicoidal composite – the reduction in the interlaminar shear stresses is the primary objective.

Table A-1. NCT304-1 Carbon/Epoxy property

Property	Value	Units
Prepreg gel temperature	300-350	ºF
Prepreg gel time	1.5	hr
Resin content	42±2	%
Tensile strength	240	ksi
Tensile modulus	18	10^6 psi
Flexural strength	245	ksi
Flexural modulus	17.6	10^6 psi
Compressive strength	128.3	ksi
Compressive modulus	17.5	10^6 psi
G_{ic} (DCB test)	2.83	(in-lb/in^2)
G_{iic} (ENF test)	7.96	(in-lb/in^2)
Poisson's ratio	0.303	Dimensionless

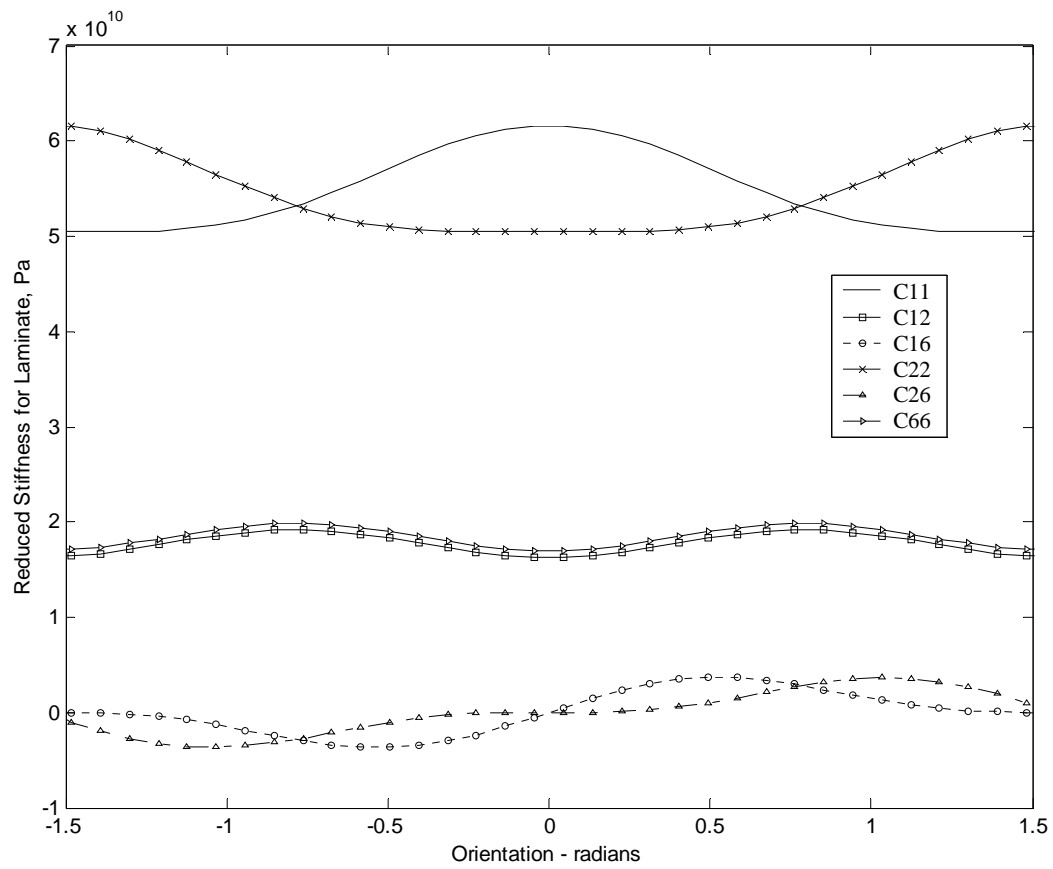All results normalized to 60% Fiber Volume

Figure A-2. Reduced stiffness matrix of the laminate as a function of orientation with respect to the global x-direction.

Appendix B. Fabrication of the helicoidal composite

A standard hand lay-up and vacuum bagging process was used for manufacturing composites. The prepreg of the composite material studied in this research was manufactured by Newport Adhesives and Composites, Inc. The nominal properties of the fiber and matrix are shown in Table A-1. The prepreg carbon-fiber epoxy NCT304-1 supplied in the form 36 inches wide continuous roll were cut to the desired size, (12 inches long by 12 inches wide), in a large shear cutter. For the helicoidal composite the stacking sequence of the specimen required 40 layers cut in the different orientations according to the desired lay-up. Therefore by using a cutting pattern corresponding to individual directions, the prepreg were cut according to the desired orientations. The next step after obtaining multidirectional cut laminas was stacking the specimen in the correct sequence. Good alignment (deviation $\pm 2°$ for the hand lay-up process) of each layer was very important because greater misalignment between the layers would change the properties of the laminate significantly. While the layers were stacked to form the laminate, trapped air bubbles were removed by rubbing the top layer with the interleaving paper simultaneously.

After obtaining the complete stacked laminate the stack was placed in a vacuum bag. The purpose of vacuum bagging is to remove air pockets and voids that could form in the composite during curing process. The stacked laminate was placed between two one-inch thick aluminum plates, and the thermocouples used to monitor the temperature distribution around the specimen plate were attached. Next, the vacuum bag was sealed by the sealant tape. Finally, the vacuum bagging assembly was inspected by connecting the thermocouples to temperature channels in the autoclave and attaching vacuum connector to the vacuum hose for inspecting the sealing system. For curing the composite, the laminate plate was placed in an autoclave and subjected to the temperature and pressure history shown in Figure B-1. The temperature and pressure cycle used in the autoclave for curing the specimen is comprised of three steps: the heat-up, curing and cool-down. According to the manufacturer's material data sheet the temperature and pressure cycle in the autoclave should be as shown in Figure B-1.
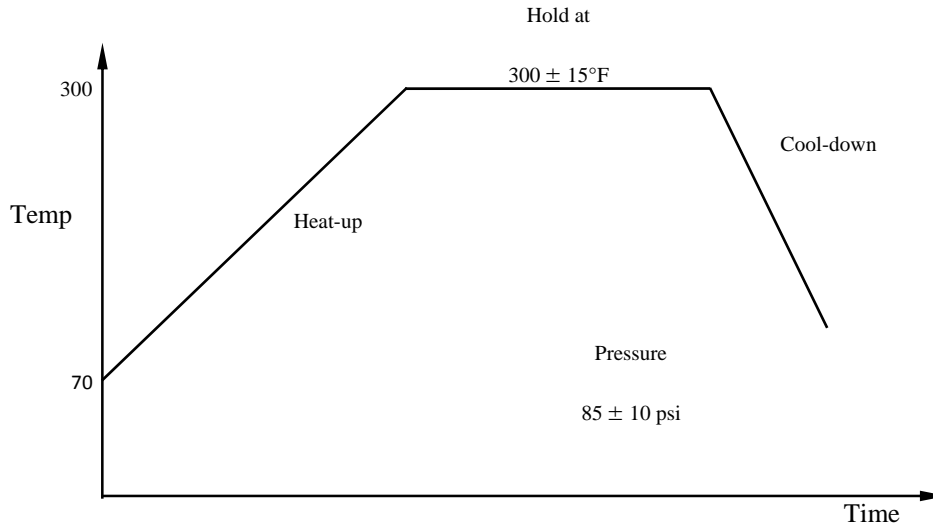
Figure B-1. Temperature and pressure cycle used for curing the helicoidal composite

For the consolidation process, the vacuum bagged assembly was located inside the autoclave chamber to heat and pressurize along the curing profile. In order to obtain good quality laminates the temperature and pressure distribution should be controlled precisely. Some preliminary tests were run to obtain the distribution of temperature gradients inside the chamber in order to determine the areas with the most uniform temperature distribution in the chamber. A few tests were also set up to monitor the thermal gradient through the thickness of the plate; in these tests six thermocouples were placed at the center of different locations to display through the thickness temperature of the quarter inch thick composite specimen as shown in Figure B-2. The pressure in the autoclave was controlled by adjusting the pressure valve to set-up the pressure corresponding to the manufacturer's recommended consolidating pressure of 85 psi. For curing laminate the temperature was increased at about 1-5°F/min until approach to the recommended curing temperature of the epoxy matrix (around 300-350°F) and maintained at the constant level for 1.5 hours. After the plate was cured, the cooling process was performed simply by turning off the power to the autoclave; the cooling rate was quite low and it took around 6-7 hours before the temperature decreased below 70°F.

```
┌─────────────────────────────────────────┐
│        TH #8: Vacuum Bag Surface          │      Vacuum
└─────────────────────────────────────────┘
┌─────────────────────────────────────────┐       Bag
│        TH #7: Aluminum Plate Top          │
├─────────────────────────────────────────┤      Aluminum plate
│              TH #6: Top                    │
├─────────────────────────────────────────┤
│            TH #5: Mid-top                  │
├─────────────────────────────────────────┤      Specimen
│            TH #4: Center                   │
├─────────────────────────────────────────┤
│           TH #3: Mid-bottom                │
├─────────────────────────────────────────┤
│             TH #2: Bottom                  │
└─────────────────────────────────────────┘      Aluminum plate
┌─────────────────────────────────────────┐
│      TH #1: Aluminum Plate Bottom          │
└─────────────────────────────────────────┘
```
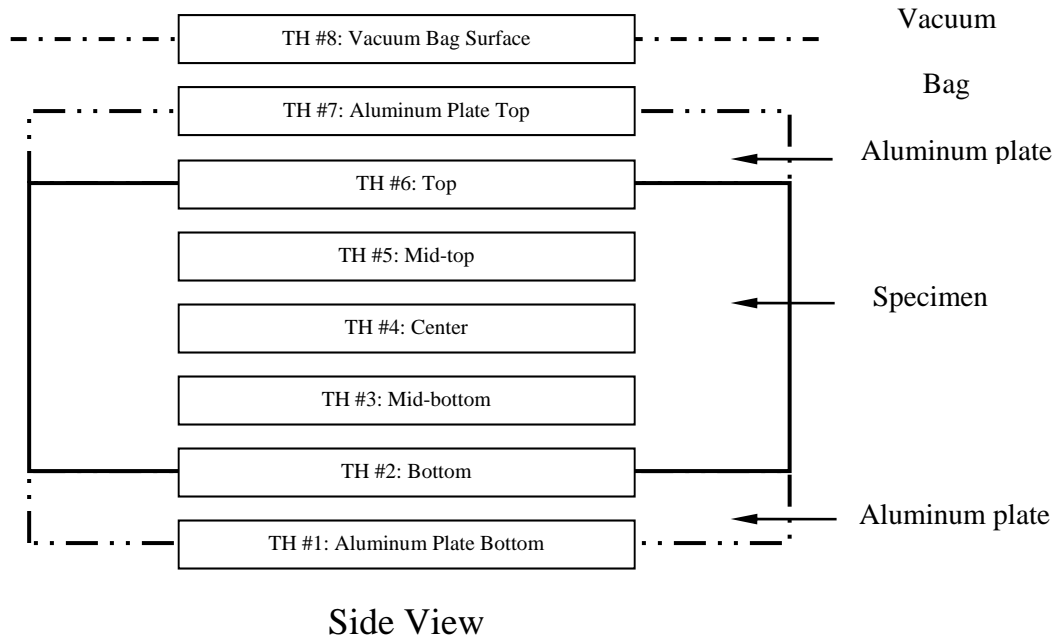
Side View

Figure B-2. Location of the thermocouples for evaluation of the through-thickness temperature distribution.

As shown in the graph in Figure B-3 the temperatures displayed by thermocouples inside the specimen and between specimen and tool plates were quite uniform. Even though there were some deviations of the specimen temperature from the set-point and the outside surface of vacuum bag during the heating cycle, the overall results were satisfactory. Thus these results provide assurance that the specimen should have an even temperature distribution during curing process. During fabrication, the temperature distribution was monitored with eight thermocouples placed in specific locations around the tool plates and the vacuum bag. After removing the cured laminate from the autoclave, an ultrasonic C-Scan was used to inspect the quality of the specimen.
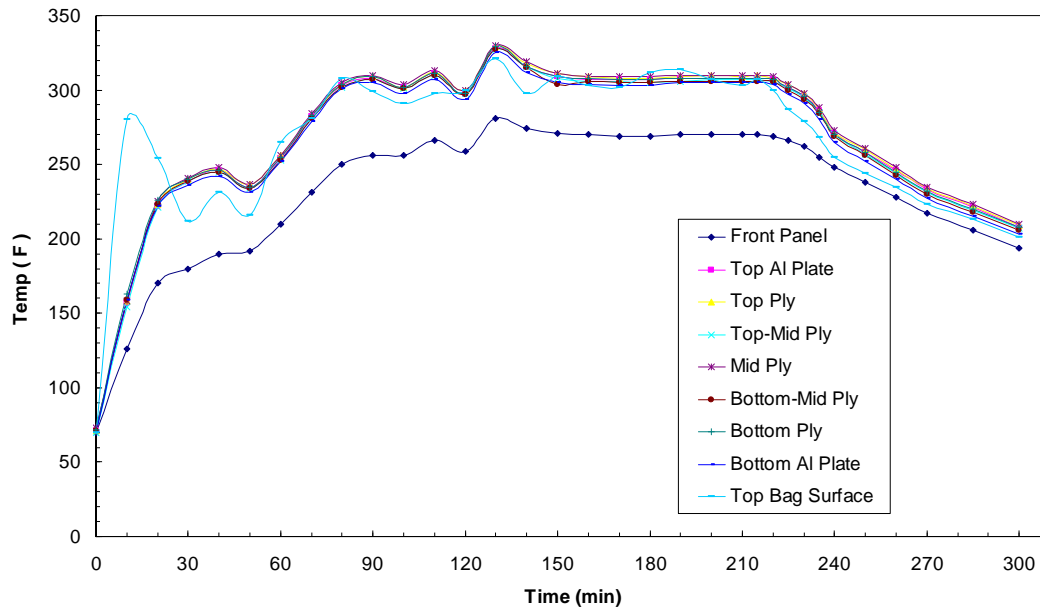
Figure B-3. Through-thickness temperature distribution in the specimen during curing monitoring locations are indicated in Figure B-2.